VILNIUS UNIVERSITY
FACULTY OF CHEMISTRY AND GEOSCIENCES
INSTITUTE OF CHEMISTRY
DEPARTMENT OF INORGANIC CHEMISTRY

Mykhailo Suleimanov
Pharmaceutical Chemistry
Master thesis

INVESTIGATION OF SUBSTITUTION EFFECTS IN LAYERED DOUBLE HYDROXIDES

Scientific advisers
Prof. habil. dr. Aivaras Kareiva
PhD student Ligita Valeikienė

_____
(permission to defend, date, signature)

Date of submission _____
Registration No. _____

Vilnius 2020

CONTENTS

INTRODUCTION

Layered double hydroxides (LDHs) also known as hydrotalcite-like systems are anion clays, recently have received increased attention due to their unique physicochemical properties [1], a wide range of applications in various fields [2] and ease of synthesis [3]. Mineral hydrotalcite with the exact formula of $[Mg_6Al_2(OH)_{16}]CO_3 \cdot 4H_2O$, was the first LDH, correctly determined by Manasse in 1915 [4]. The main structural features were explained later in the 1960s by Allman [5] and Taylor [6]. The general formula of an LDH is defined as $[M^{2+}_{1-x}M^{3+}_x(OH)_2]^{x+}(A^{m-})_{x/m}] \cdot nH_2O$, where M^{2+} and M^{3+} are divalent and trivalent metal cations with similar radii and A^{m-} is an interlayer anion [7]. The nature and proportions of cations can be varied [8,9].

There are many approaches to synthesize different LDH materials: sol-gel, urea hydrolysis, hydrothermal synthesis, anion-exchange, combustion and electrochemical synthesis, synthesis using microwave irradiation and coprecipitation method [1,10]. Although one of the main common ways for the synthesis of LDHs is coprecipitation synthesis [1,10], alternative sol-gel method shows some advantages over that one: the higher specific surface area of LDH [11], high homogeneity [12] simplicity, effectiveness, and cost-efficiency [13]. Calcination of LDHs leads to a collapse of layered structure and formation of mixed metal oxides (MMO), which possess high surface area and could be utilized as catalysts [14]. In turn, MMO, when exposed to aqueous solutions, are restored into LDH, what is known as "memory effect" [15]. Regeneration of layers is widely used for intercalation of desired anions into the structure of LDH [10]. A large variety of anions can be incorporated between hosts layers as LDHs have a significant feature of tremendous anion exchangeability. Host lattice chemical, electronic, optical, and magnetic properties can be drastically changed by such intercalation reactions [8].

Other routes of modifying LDH structure can be accomplished by changing their surface zone, assembling hybrids, and regulating layer composition, size and morphology [16]. Incorporation of metal ions into the LDH lattice is used to control the size and morphology of LDH particles [17] and enhance its catalytic activity [2]. However, the addition of new improper metal components into the LDH framework may inhibit LDH performance [18]. Manipulation of layer composition by introducing metal ions into LDH structure allows tuning of morphological features and surface properties of LDHs [16].

A possibility to synthesize a large number of various compositions and metal-anion combinations is one of the main prevalences of LDH among other layered materials [7]. LDHs are emerging materials as environmental remedies, especially in water systems [19]. Functionalized LDHs can provide not only physical but also chemical means to remove contaminants, which makes them advantageous over other materials such as activated carbons and silicates [16]. Due to versatile features, LDHs can be applied in various fields as cellular delivery agents [20], sorbents [21], or catalysts [4]. Designed and fabricated mixed-metal LDH materials with intercalated anions possess valuable properties and have a potential to be applied in various areas as catalysts, adsorbents, precursors for drug delivery systems or nanomaterials and in other environmental and biomaterial related fields.

The first aim of this work was to fabricate $Mg_{2-x}M_x/Al_1$-LDH (M = Ca, Sr, Ba) and related MMO by the sol-gel method and characterize the synthesis products by using X-ray powder diffraction (XRD) analysis, Fourier-transform infrared spectroscopy (FT-IR), BET and BJH methods and scanning electron microscopy (SEM). Another purpose of this thesis was to investigate the possibility of intercalation of organic species into $Mg_{2-x}M_x/Al_1$-LDH (M = Ca, Sr, Ba) structures.

1. LITERATURE OVERVIEW

1.1 Structural peculiarities

Layered double hydroxides are a group of brucite-like layered materials. They consist of positively charged host layers and guest interlayer anions, which are assembled by the non-covalent bond interaction [22]. Their compositions are commonly described by the general formula $[M_{1-x}^{2+}M_x^{3+}(OH)_2]^{x+}A_{x/z}^{z-}\cdot mH_2O$, in which M^{2+} and M^{3+} are divalent (Mg^{2+}, Zn^{2+}, Co^{2+}, Fe^{2+}, Ni^{2+}, *etc*.) and trivalent (Al^{3+}, Cr^{3+}, Fe^{3+}, *etc*.), A^{z-} is an interlayer anion, x value is the surface charge, determined by the ratio of the two metal cations, which is subject to change for various applications and is usually ranging 0.2 to 0.4 depending on the nature of the metal cation.[23]. Sometimes M^{2+} cation can be substituted by Li^+ and M^{3+} cation by M^{4+} cations [24]. Each cation is octahedrally surrounded by six perpendiculars to layers OH^- ions, and these octahedral units share edges to form a 2D layer (**Fig. 1**) [7,25].

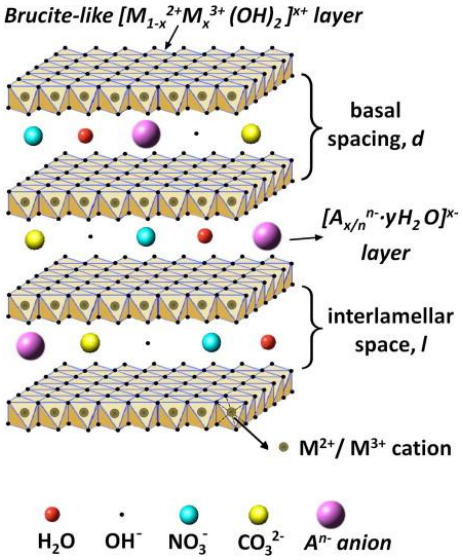

Fig. 1. Schematic structure of LDH compounds with possible anionic hosts in the interlayer space. Adapted from D. Scarpellini et al./Microelectronic Engineering, 126, (2014), 129–133.

Replacement of M^{3+} cations of a similar ionic radius to M^{2+} produces a positively charged framework, hence anions present between the layers to balance the positive charges of the hydroxide layers [10,19]. The most common ways brucite-like layers can be stacked are rhombohedral (3R symmetry) and hexagonal (2H symmetry) [26]. The rhombohedral cell consists of three metal hydroxide slabs and the hexagonal cell comprises of two [27]. The local geometry at the metal (D_3d) is strongly distorted away from the idealized (Oh) arrangement because of compression of the octahedra along the stacking axis. This distortion results in hexagonal symmetry (space group P3m1) [4,28]. Pristine LDHs comprise intercalated CO_3^{2-} ions, which lie parallel to the hydroxide layers to enable close contact between the oxygen atoms and the layer by forming hydrogen bonds sheets [29]. The carbonate-LDHs crystallize in the structure of the $3R_1$ polytype. Molecular symmetry of the carbonate ion (D_{3h}) matches the local symmetry of the interlayer sites in the $3R_1$ polytype, also (D_{3h}). Consequently, hydrogen bonding between the layer hydroxyl and interlayer carbonates is maximized [30]. The interlayer region also contains water molecules and the amount of water is determined by the nature of the interlayer anions, the water vapour pressure and temperature [8]. Brucite layers and anions are connected to water molecules through the ionic bonding, hydrogen bonding, and van der Waals forces [28]. LDH materials with many different anionic species intercalated have been reported

such as Cl^-, F^-, CO_3^{2-}, NO_3^- and SO_4^{2-} [31]. There are no strict limitations regarding the nature of the interlayer anions. However, anions with low charge and big size are unable to balance the positive charge in the layers [7,32]. An important characteristic of the LDHs is the lack of crosslinking between the cation layers which enables the interlayer spacing to exfoliate or contract to host a large variety of interlayer anions [33,34]. LDHs have an unusual affinity toward carbonate ions owing to their ability to hydrogen bond with the metal hydroxide layers [35]. There is a large number of possibilities to vary the cation site as well as the anion introduction into the interlayer space between hydroxide structures without altering the structure of the LDH, hence to compose materials with diverse physicochemical properties [36,37].

When LDHs are heated at temperatures between 250 and 650 °C, dehydration, and loss of interlayer anions occur which leads to the collapse of the layered structure. This process is known as calcination [23]. The calcination significantly improves the adsorption capacity of the hydrotalcite resulting in higher surface area and thermally and chemically stable calcined clays with a higher number of active sites [38]. The temperature of calcination depends on the composition of the LDH precursor [28]. After calcination, LDHs is changed into amorphous mixed metal oxides (MMO) [19]. The MMO have a very high surface area with several basic sites and exhibit high catalytic activity [35]. They were reported as efficient energetics of CO_2 uptake [39]. When MMO are exposed to an aqueous solution of an anion, they restore to the original layered structure with a desired intercalated anion. This phenomenon was named as ‘‘memory effect‘‘ (**Fig. 2**) [40].

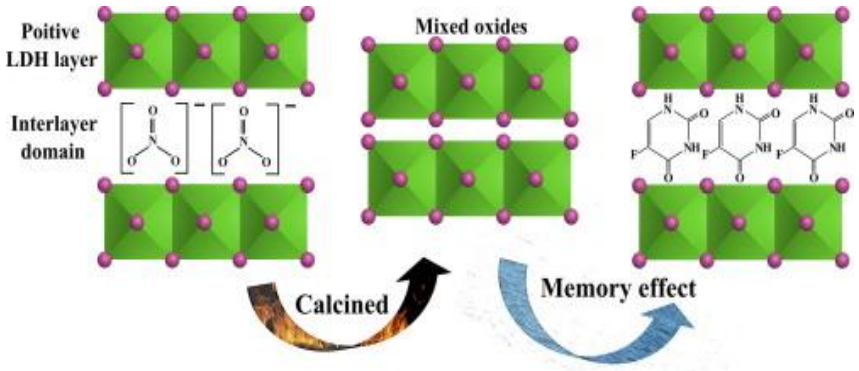

Fig. 2. Mg/Al LDH loaded with 5-fluorouracil (5-FU) via memory effect. Adapted from F. Peng et al./Materials Letters, 213, (2018), 383–386.

The anions incorporated do not necessarily need to be the anion that was in the original LDH material, and hence this is an important method to obtain various inorganic and organic anion forms of LDHs [25]. Reconstruction of the structure is very difficult if LDH has been calcined at too high temperature [41]. The reconstruction process should be carried out under an inert nitrogen atmosphere when an anion other than carbonate is to be incorporated [28].

1.2 Methods of synthesis

Synthetic method plays an important role in modelling the surface properties of the layered double hydroxides [12,42]. Although LDHs occur naturally as hydrotalcite, they can be readily fabricated in the laboratory. The preparation approach defines such characteristics as the phase purity, composition and physio-chemical properties of LDHs [37]. There is a need in a cheap and effective method of fabricating materials for industrial and scientific aims [43]. Therefore, this chapter introduces a review on some of the main synthetic routes of LDHs and their recent advances.

Depending on the goals and requirements LDHs can be fabricated by various methods. One of the main methods of choice to fabricate LDH platelets is coprecipitation method [10]. The process of

coprecipitation is the most favoured as it is easy to conduct and it does not require any unstable solvents or other costly chemicals or equipment [44]. By this method, LDHs are obtained using simultaneous drop-wise addition at constant pH of aqueous solutions of alkali and mixed M^{2+}/M^{3+} salts containing the desired interlayer anion if different from that in the metal salt precursor [45]. The intercalated host-guest compound is synthesized directly from the salts in the coprecipitation process since the special preparation stage builds up the layered hosting system and distributes the anionic guests in the interlayer space [46]. Two coprecipitation techniques are commonly used: precipitation at low supersaturation, and precipitation at high supersaturation [25,47]. The supersaturation state is required to enable the simultaneous precipitation of two or more cations [28]. The conditions of supersaturation are reached by regulating the solution's pH [25,48]. The pH duration of the reaction can be either held constant during precipitation by adding an alkaline solution or varied [46]. Precipitation at low supersaturation is performed by slow addition of mixed solutions of divalent and trivalent metal salts to the aqueous solution of the desired interlayer anion. The second solution of an alkali is added into the reactor simultaneously at such a rate as to maintain the pH at a selected value leading to the coprecipitation of the two metallic salts [25]. At high supersaturation mixed M^{2+}/M^{3+} salt solution is added to an alkaline solution containing the target interlayer anion under intensive agitation, which leads to a continuous change in solution pH value, followed by an ageing step [28]. Although LDHs prepared at high supersaturation conditions are easy to fabricate [47], the products obtained by coprecipitation at low supersaturation are typically more crystalline and allows the control of the charge density of ($M^{2+/}M^{3+}$ ratio) of the hydroxide layers of the resulting LDH by regulating the solution pH [46,49]. Crepaldi et al. compared materials obtained by both methods with or without hydrothermal treatment and found that LDHs with better crystallinity and higher specific surface area was generated by coprecipitation at a constant pH [50]. A thermal treatment process after coprecipitation is often necessary to increase yields or the crystallinity of amorphous or poorly crystallized materials. Other factors that influence on the structure are temperature, ageing, the nature of anions [28]. Coprecipitation is widely used for direct one-pot synthesis of LDHs containing a variety of layer cations and interlayer anions [50]. In attempt to prepare stabilized pigments coprecipitation method was used to intercalate perylene chromophore into LDH [51]. H. Zhang et al. investigated that the chance of carbonate contamination is lowered using this approach [52]. Moreover, this method is optimal for scaling up to manufacture large volumes of material [25].

The sol-gel method is well-known for being an effective method, by which LDHs are fabricated possessing high purity [47]. During the sol-gel method, LDHs are made by the gradual conversion of a liquid phase (sol) obtained by a colloidal suspension of the desired metal precursors such as inorganic salts or metal-organic into a polymer solid (gel) phase [46,47]. A gel is a wet solid-like material in which a nanostructured solid network is dispersed in the liquid medium [53]. As mentioned before, this approach produces highly pure LDHs compounds. For instance, recently Bi-substituted LDHs were synthesized by sol-gel method and gave the single phase of $Mg_3Al_{1-x}Bi_x$ ($x \leq 0.2$), while the side $Bi_2O_2CO_3$ phase occurred during the synthesis by coprecipitation method [12,54]. Furthermore, Valente et al. found that crystallinity depends mostly on the reconstruction condition, and crystal sizes do not necessarily decrease from the as-synthesized to the reconstructed LDHs [15]. By the sol-gel method, better homogeneity can be achieved due to molecular-level mixing of the precursors [13,53]. It is possible to alter the morphological properties of sol-gel LDHs in a convenient way by changing the cation and anion species [47,55]. The sol-gel hydrotalcite is also known to exhibit thermal stability [55]. Besides, the sol-gel method allows surpassing the Mg/Al ratio limit within the range 1.5–3.0, which is typical for coprecipitation synthesis [46,56]. Sol-gel technique is commonly used for the synthesis of metal oxide nanoparticles and mixed oxide materials [19]. Recently G. Fetter et al. researched a way to enhance high surface area and purity of

hydrotalcite-like compounds by using microwave irradiation during the gelling and crystallization steps in sol-gel method [57]. Compare to other methods as the coprecipitation method, the sol-gel technique shows a higher specific surface area [58]. However, if metal alkoxides in the sol-gel method are used as precursors, the synthesis conditions should be more strictly controlled than in the co-precipitation method [59]. This drawback can be overcome by usage of alkoxide-free sol-gel method, which is reported to be a great alternative approach, as it is not based on using hazardous and costly materials and solvents. Furthermore, this environment-friendly technique can be upscaled for the removal of toxic arsenic species for water treatment [43,53].

Alternatively, LDHs can be synthesized by the urea method. Hydrolysis of metal cations ruled by urea decomposition is a gentler and slower process of hydroxide formation than neutralization by alkalis [53]. Compared with the conventional method of coprecipitation, the urea hydrolysis method allows metal ions to homogenously precipitate which could assist in the formation of large and highly crystallized layered double hydroxide at the micrometre scale [60]. The particle size, crystallinity level and uniformity depend on the reaction temperature, which defines the hydrolysis rate of urea. As a result, larger particles are formed at lower temperatures, because of the nucleation rate, while at high temperatures, particle sizes are smaller and more uniform [28,47].

The anion-exchange method is based on the exchangeable properties of the interlayer anions. This method is especially useful when the coprecipitation method is inapplicable such as when, the divalent or trivalent metal cations or the anions involved are unstable in alkaline solution, or the direct reaction between metal ions and guest anions is more favourable, or there is no suitable soluble salt of the guest anions [28]. LDH exists in nature in its carbonate form, which shows quite a low affinity for the exchange reactions compared to monovalent ions [61]. The host-guest exchange generally depends on the electrostatic forces between positively charged LDH layers and the exchanging anions. Hence anions can be easily replaced by target anions with higher electrostatic interaction with layers [62]. To perform the anion exchange the nature of the counterion originally present in the LDH should be considered. Anions with higher negative charges tend to exchange and replace those with lower charge in the interlayer spaces [25,46]. The ion-exchange ability of common incoming anions is as follows:

$$CO_3^{2-} > HPO_4^{2-} > SO_4^{2-}; OH^- > F^- > Cl^- > Br^- > NO_3^- > I^-$$

Therefore NO_3^- or Cl^- intercalated LDHs are usually used as the precursors for ion exchange [28]. The preparation of hydrotalcite-like Mg/Al hydrotalcite-like compounds was also mentioned by the synthesis of combustion, electrochemical, and microwave irradiation. The limitations of these suggested techniques are that materials have low crystallinity, time-consuming processes and rather costly. Besides, it may cause a large number of surface defective sites [59]. Hydrotalcite prepared from different routes is expected to offer flexibility for further improvement and use in a wider scope of applications [47]. Despite the large variety of synthetic methods for fabrication of LDHs, yet there is a difficulty to scale-up the production of materials needed for the technological application. Recently more attention is paid towards the development of fast and green preparation approaches of LDHs [46].

1.3 Functionalization of layered double hydroxides

Functionalization of LDHs aims to modify their shape, size, composition, the introduction of foreign species into LDHs to create and develop new exciting properties [63]. One of the common techniques for modifying LDHs is intercalation [64]. Intercalation reactions are important, as they can be used to significantly alter a host lattice's chemical, electrical, optical and magnetic properties [8]. Introduction of guest species into interlayers can increase catalytic activities of LDH

materials [24]. Factors that should be taken into account when intercalating guest species into LDH structure are the number (monolayer, bilayer), size, the orientation of the guest as well as the interactions between the negatively charged guest and positively charged host [65]. For instance, decavanadate anion $[V_{10}O_{28}]^{6-}$ was successfully intercalated into LDHs by the ion exchange method (**Fig. 3**).

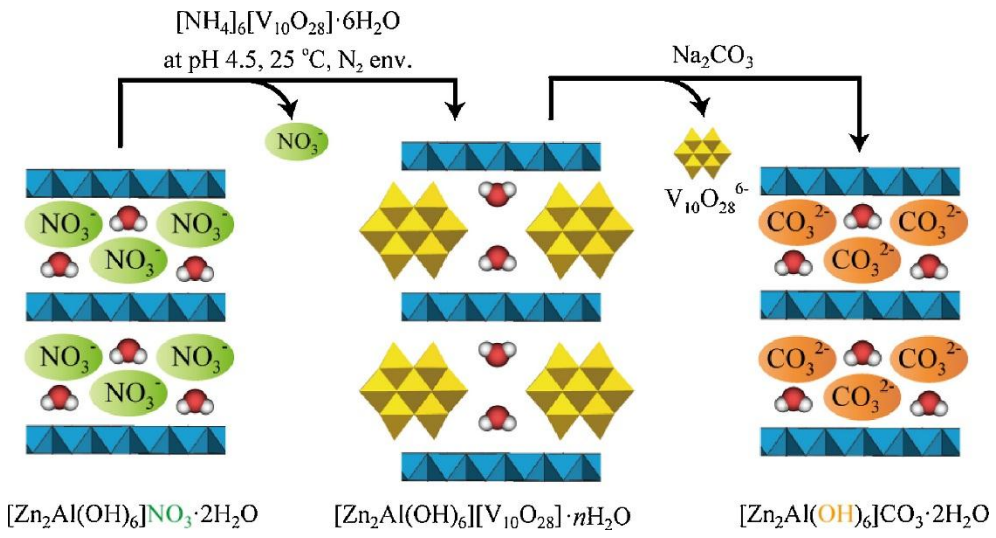

Fig. 3. Schematic representation of intercalation of $[V_{10}O_{28}]^{6-}$ anion into ZnAl-LDH through ion exchange synthetic route. Adapted from S. Omwoma et al./Coordination Chemistry Reviews, 258–259, (2014), 58– 71.

Various drugs can be incorporated into LDHs via intercalation technique [66]. It usually leads to improvement of the solubility of the drugs, without modification of their chemical structure, thus enhancing its bioavailability [67]. Another additional valuable feature of a drug-LDH intercalation compound is an ability for drug controlled release [68]. Recently, Amoxicillin antibiotic of the penicillin group was successfully intercalated into the interlay space of the ZnAl-LDH as a monolayer, by using a calcination–reconstruction method [69].

The addition and elimination of metal components, or the substitution of metal components with other metals determine the properties of LDHs [70]. The introduction of the optimum number of cations into the host layers of the LDH increase the net positive charge in the brucite-like sheet. Thus, by such modification, layer charge density is increased, which subsequently enhance the anion exchange capacity of the LDHs [37].

One of the most important factor to consider when modifying layer composition is ionic radii of the two metal cations [4]. The most common naturally occurring LDH contains Mg^{2+} and Al^{3+} [29]. Recently, incorporation of Co^{2+} into MgAl-LDH via a soft chemical hydrothermal reaction was reported. No impurity phase was observed as well as crystallinity, particle size, and morphology of pristine LDH were preserved during the substitution reaction [2,17]. Furthermore, by modifying the size of the particle Zhao et al. synthesized NiTi-LDH monolayer nanosheets with high specific pseudocapacitance [71]. Moreover, tuning the molar ratio of metal components of LDHs greatly influences their catalytic activity [2,72]. Other common ways of regulating physical properties of LDH by functionalization include surface modification [73] and hybridization with other materials [38].

1.4 Applications

Due to inherited properties, LDHs show great potential in a wide range of applications such as environmental, energy, catalysis, and biomaterials related fields [24,74]. Layered double hydroxides can be used in various applications in the pharmaceutical industry [74]. LDHs possess high surface area, memory effect, high anion exchange capacity and stable physicochemical properties, hence they have been widely investigated as drug delivery systems [75–77]. Such hydrotalcite-like materials possess several advantageous as good biocompatibility [20], controlled release of drugs [66] and low cytotoxicity [62]. For instance, Cefazolin, the antibacterial agent of the cephalosporin class, has been intercalated into layered double hydroxide by ion-exchange reaction [78]. Results reported increased release property and chemical stability of Cefazolin-LDH nanohybrid, it also showed enhanced antibacterial activity compared to cefazolin itself. Moreover, the release of anionic drugs can be controlled in a passive way by selecting a proper pH [20]. When released, the LDH composite is exposed to various pH conditions so that at the appropriate pH, the composite breaks slowly releasing the drug at the correct location [62,76]. Another problem that drug companies deal with is poor solubility of active ingredients. The addition of LDHs can improve the solubility of the drugs [77]. Gliclazide is a poorly water-soluble drug which is used in the treatment of type II diabetes mellitus. Its adsorption is limited, due to poor solubility [79]. The gliclazide-hydrotalcite-like clay nanohybrid has been developed via ion-exchange approach and showed significant improvement of the solubility and dissolution rate in comparison to the crystalline drug. Moreover, LDH can be used in photodynamic therapy for treating cancer. Introduction of zinc phthalocyanine (ZnPc) into the interlayer space of LDH nanoparticles resulted in high singlet oxygen production efficiency, enhanced photostability, good biocompatibility and low cytotoxicity [80]. Although, LDH nanoparticles are promising gene and drug delivery systems and can be effective *in vitro* in providing sustained release of drugs, yet they are facing certain problems as short half-life when tested *in vivo* [81]. For the application of such materials in pharmaceutical industry reproducibility of LDH nanostructures with small variation in size, thickness, and geometry and stability have to be sustained [80]. Other biomedical applications of LDH materials include biosensing and antibacterial materials [7].

LDHs possess specific surface area, porosity and a large number of active sites available, which allow to apply hydrotalcite-like materials for removal of toxic metals and ions from water and also from the atmosphere through adsorption [31]. During the surface adsorption, water contaminants adhere to the surface of the LDH material [62]. Recently, Pshinko reported the use of $[Zn_4Al_2(OH)_{12}]\cdot CO_3\cdot 8H_2O$ layered double hydroxide as an effective adsorbent for toxic heavy metals removal from aqueous media [82]. Furthermore, the possibility to modify adsorption sites as layer charge density, pore structure at micron-nano scale allows tuning the active structure and adsorption kinetics for a specific adsorption process [16]. Lately, Asiabi et al. developed layered double hydroxides intercalated with the diphenylamine-4-sulfonate for extraction of heavy metals from water **(Fig. 4**) [83]. Results showed that the adsorption of these metal ions occurred mainly through interaction with interlayer anions. Selectivity and efficiency of removal of pollutants can be enhanced by the introduction of functional intercalants into LDH and it depends on the structure of the interlayer anion. Besides, anionic clays were investigated for immobilization and removal of radioactive pollutants [22,84], slow release of fertilizers [85], and reduction of nitrogen oxides [86].

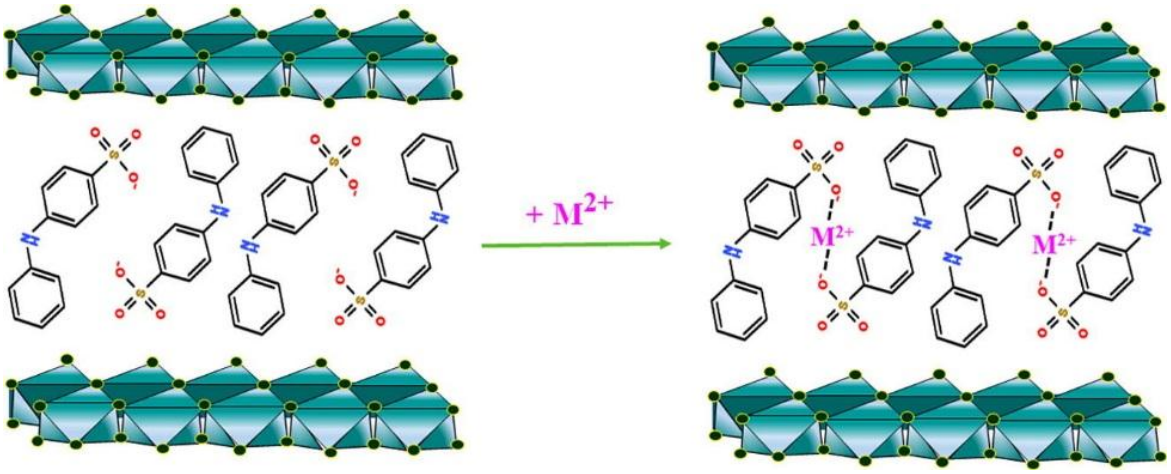

Fig. 4. Removal of heavy metals by layered double hydroxides intercalated with the diphenylamine-4-sulfonate. Adapted from H. Asiabi et al./Chemical Engineering Journal, 323, (2017), 212–223.

Owning to unique structure, composition diversity, high stability LDHs are applied as supports for catalytic oxidation and hydrogenation reactions. A uniform distribution of cations, and strong interaction between the active component and the support increase catalytic activity and stability of LDH materials [87]. LDH based composites are known for being great photocatalysts for environmental remediation due to their non-toxicity and stability [19]. For example, recently Jo et al. synthesized Ag/LDH/g-C_3N_4 nanocomposite by an *in situ* hydrothermal method [88]. The LDH-based nanomaterial exhibited remarkable photocatalytic activity for the photodegradation of aqueous organic pollutants and showed photostability with no significant change in photodegradation rate even after several catalytic runs.

Layered double hydroxides are widely investigated as potential materials for supercapacitors, owing to their ideal redox behaviour, environmental friendliness and comprehensive utilization of homogeneously dispersed transition metal sites [71,89]. NiCoAl-LDH nanoplates coupled with NiCo-CH nanowires have been fabricated *in situ* on graphite paper by hydrothermal method. Such composite serves as an asymmetric supercapacitor, which exhibits a long cycle life, high energy density and power density [90].

2. EXPERIMENTAL

2.1 Materials

Aluminium nitrate nonahydrate ($Al(NO_3)_3 \cdot 9H_2O$, 98,5%, Chempur), magnesium nitrate hexahydrate ($Mg(NO_3)_2 \cdot 6H_2O$), 99,0% Chempur), calcium nitrate tetrahydrate ($Ca(NO_3)_2 \cdot 4H_2O$, 99%, Chempur), strontium nitrate ($Sr(NO_3)_2$, 99,0%, Chempur) and barium nitrate ($Ba(NO_3)_2$, 99,0%, Chempur) were used as starting materials in the preparation of alkaline earth metal substituted LDHs. Citric acid monohydrate ($C_6H_8O_7 \cdot H_2O$, 99,5%, Chempur) and 1,2-ethanediol ($C_2H_6O_2$, 99,8%, Chempur) were used as complexing agents in the sol-gel processing. Ammonia solution (NH_3, 25%, Chempur) was used to change the pH of the solution. Hydrochloric acid (HCl, 37%, Sigma-Aldrich), potassium sodium tartrate tetrahydrate ($KNaC_4H_4O_6 \cdot 4H2O$, 99%, Chempur), sodium chloride (NaCl, 99,5%, Sigma-Aldrich) and tri-sodium citrate dihydrate ($C_6H_5O_7Na_3 \cdot 2H_2O$, 99,5%, Chempur) were used for the anion exchange experiment. All reagents were used as received without further purification.

2.2 Synthesis of Mg-Al non-substituted and alkaline earth metal-substituted LDHs and derived MMO by sol-gel method

For the synthesis of $Mg_{2-x}M_x/Al_1$ (M = Ca, Sr, Ba, x = 0.01-0.05) layered double hydroxides stoichiometric amounts of starting materials were dissolved in distilled water under continuous stirring. Dissolved citric acid was added to the above solution and the obtained mixture was stirred for 1 h at 80 °C. 2 ml of 1,2-ethanediol was then added to the resulting solution. The obtained transparent gels were obtained by the complete evaporation of the solvent under continues stirring at 150 °C. The synthesized precursor gels were dried at 120 °C for 24 h. The mixed metal oxides (MMO) were obtained by calcinating the gels at 650 °C for 4 h. Reconstructed LDHs were obtained by dispersing MMO in water under continuous stirring for 6 h at 50 °C and changing the pH of the solution to 10 with ammonia. After mixtures were dried for the following 24 h at 80 °C. The resulting precipitates were filtered, washed several times with water and acetone and dried.

2.3 Modification of LDHs

2.3.1 Intercalation of chloride anions into Mg-Al non-substituted and alkaline earth metal-substituted LDHs by anion-exchange

The 0.5 g of $Mg_{2-x}M_x/Al_1$-LDH was added into 500 mL of the aqueous solution of NaCl (0.5 M), following by 3.3 mM of HCl. The solution was stirred for 24 h at ambient temperature. The obtained precipitates $Mg_{2-x}M_x/Al_1$-LDH-Cl were filtrated, washed several times with distilled water and acetone, then dried and collected.

2.3.2 Intercalation of tartrate and citrate anions at different temperature and pressure conditions by anion-exchange

The $Mg_{2-x}M_x/Al_1$ (M = Ca, Sr, Ba) LDHs with different interlayer anions were prepared through a further anion exchange process using the obtained LDH-Cl as a precursor. LDH-Cl precursors (2 mmol) were dispersed in the decarbonized water with 1,5 molar excess amounts of the salts of the desired anionic species ($KNaC_4H_4O_6 \cdot 4H_2O$ and $C_6H_5O_7Na_3 \cdot 2H_2O$). The mixture was stirred for the

following 24 h at ambient temperature. The resulting precipitates $Mg_{2-x}M_x/Al_1$-LDH-tartrate and $Mg_{2-x}M_x/Al_1$-LDH-citrate were filtered, washed several times with water and acetone and dried. The same intercalation experiment was performed under hydrothermal conditions using a thermobomb (at 100 °C for 24h).

2.4 Characterization technics

X-ray diffraction (XRD) analysis of specimens was performed using a MiniFlex II diffractometer (Rigaku) (Cu K_α radiation) in the 2θ range from 10 to 70° (step of 0.02°) with the exposition time of 2 min per step. The morphological features of LDH samples were estimated using a scanning electron microscope (SEM) Hitachi SU-70. To determine the surface area and pore diameter of the materials nitrogen adsorption by the Brunauer, Emmet and Teller (BET) and Barret (BJH) methods were performed using TristarII. Fourier-transform infrared spectroscopy (FT-IR) spectra were recorded using Bruker-Alpha FT-IR spectrometer (Bruker) in the range of 4000–400 cm^{-1}.

3. RESULTS AND DISCUSSION

3.1 Characterization of alkaline earth metal-substituted Mg-Al layered double hydroxides and derived MMO obtained by sol-gel synthesis

Fig. 5 shows XRD patterns of sol-gel derived $Mg_{1.98}Ca_{0.02}/Al_1$ LDHs reconstructed by changing the pH of the solution from 10 to 12. 1% mol of calcium could be introduced easily instead of magnesium to Mg_2Al_1 LDHs without destroying the layered structure. However, a minor amount of alumina and magnesium oxide phase is also forming during the reconstruction approach. And the amount of magnesium oxide phase monotonically increased with increasing pH of the solution from 10 to 12. Besides, the reflections of LDHs were most intensive in the case when the reconstruction of sol-gel derived mixed-metal oxides (MMO) was performed at pH=10. Therefore, further syntheses of LDHs with higher amount of calcium were conducted using the lowest value of pH 10.

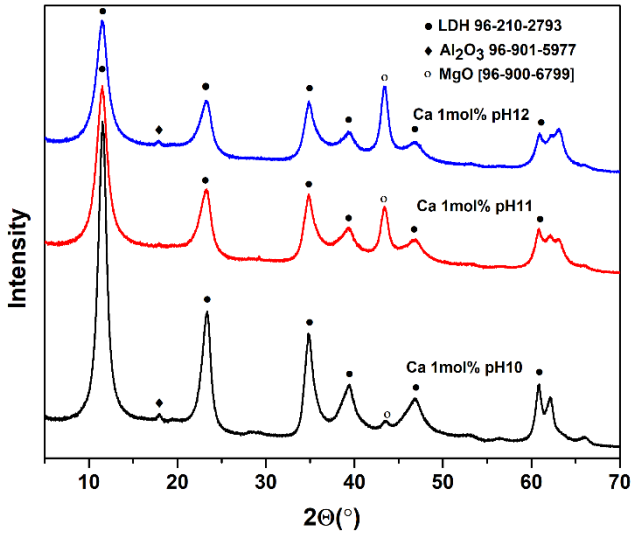

Fig.5. XRD patterns of sol-gel derived $Mg_{1.98}Ca_{0.02}/Al_1$ LDHs obtained at different pH.

The XRD patterns of MMO obtained by heating the $Mg_{2-x}Ca_x/Al_1$ LDHs precursor gels at 650°C are presented in **Fig. 6.** Thermal treatment of an LDH at elevated temperatures results in loss of interlayer water molecules, charge-compensating anions and dehydration of brucite-like layers. The XRD patterns of synthesis products with a different substitutional level of Ca are almost identical and revealed in all cases the formation of poorly crystalline magnesium oxide Mg(Al)O (reflections at 2θ angles ≈ 36, 43.5, 63.5).

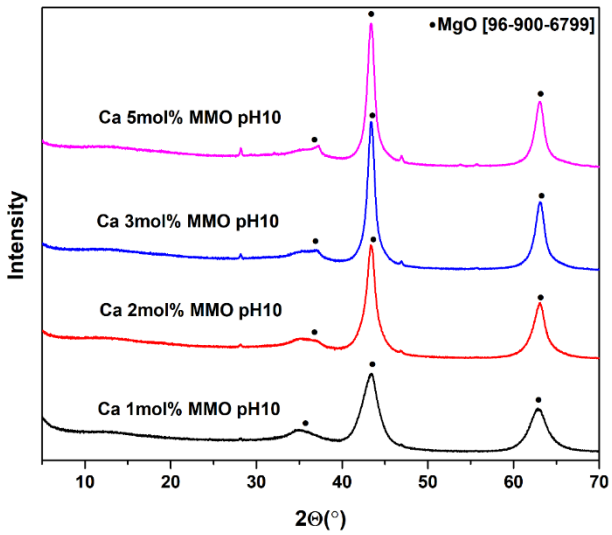

Fig. 6. XRD patterns of mixed-metal oxides (MMO) obtained by heating the $Mg_{2-x}Ca_x/Al_1$ precursor gels at 650 °C.

However, the phase purity of sol-gel derived $Mg_{2-x}Ca_x/Al_1$ LDHs evidently is dependent on the amount of introduced calcium (**Fig. 7**). With an increasing amount of Ca up to 5% mol, the intensity of characteristic reflections of LDHs monotonically decreases in the XRD patterns, and the amount of impurities, such as Al_2O_3, $CaCO_3$ and magnesium oxide phase slightly increased.

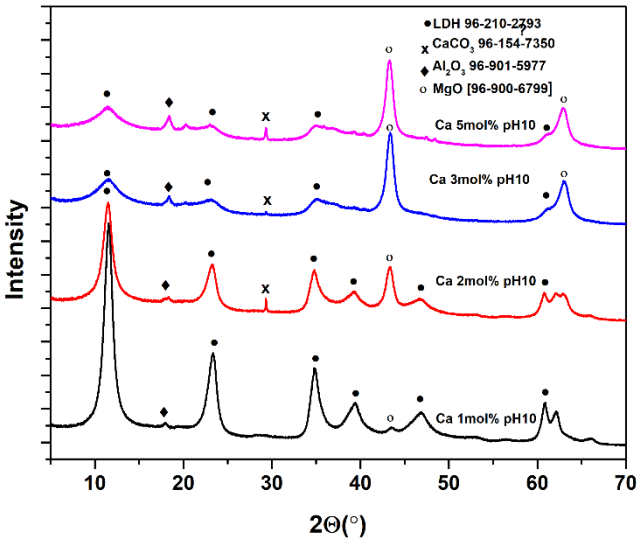

Fig. 7. XRD patterns of the sol-gel derived $Mg_{2-x}Ca_x/Al_1$ LDHs.

Fig. 8 shows XRD patterns of $Mg_{1.98}Sr_{0.02}/Al_1$ LDHs obtained by sol-gel reconstruction approach at different pH. The phase purity of $Mg_{1.98}Sr_{0.02}/Al_1$ contrary to $Mg_{1.98}Ca_{0.02}/Al_1$ LDHs is independent on the value of solution pH. The formation of LDHs phases along with impurities of Al_2O_3, $SrCO_3$ and magnesium oxide phase is evident from XRD patterns in all cases. So, to have more comparable results, the synthesis of $Mg_{2-x}Sr_x/Al_1$ precursor gels with different amount of strontium was performed also at pH = 10.

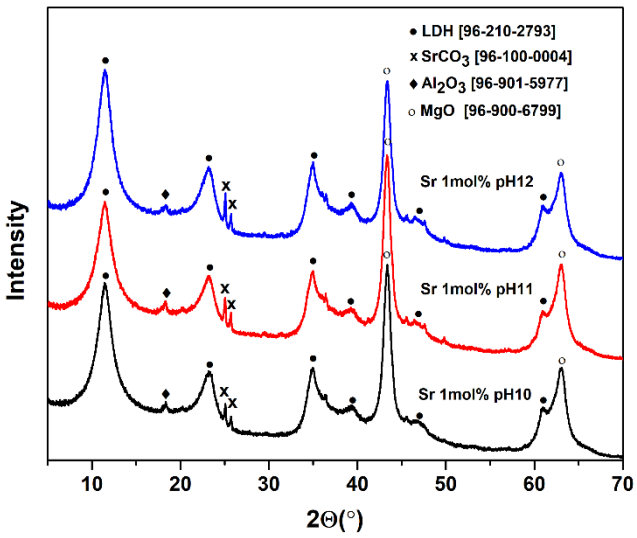

Fig. 8. XRD patterns of sol-gel derived $Mg_{1.98}Sr_{0.02}/Al_1$ LDHs obtained at different pH.

The XRD patterns of two MMO obtained by heating the $Mg_{2-x}Sr_x/Al_1$ LDHs precursor gels at 650°C are depicted in **Fig. 9**. As seen, the synthesis product of the heat-treated sample with 5% mol of Sr contains a high amount of crystalline $SrCO_3$. The phase purity of sol-gel derived $Mg_{2-x}Sr_x/Al_1$ LDHs also is dependent on the amount of introduced Sr. It can be concluded from the results presented in **Figs. 9 and 10**, that $SrCO_3$ does not undergo the reconstruction. The formed $SrCO_3$ during the formation of MMO remains in the sol-gel derived LDHs.

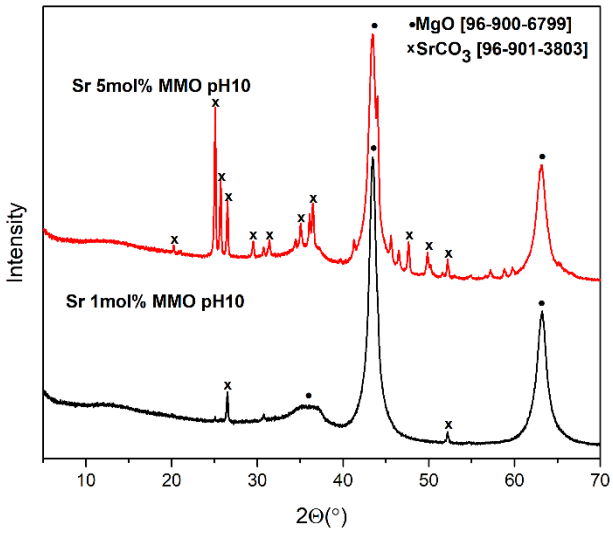

Fig. 9. XRD patterns of mixed-metal oxides (MMO) obtained by heating the $Mg_{2-x}Sr_x/Al_1$ precursor gels at 650 °C.

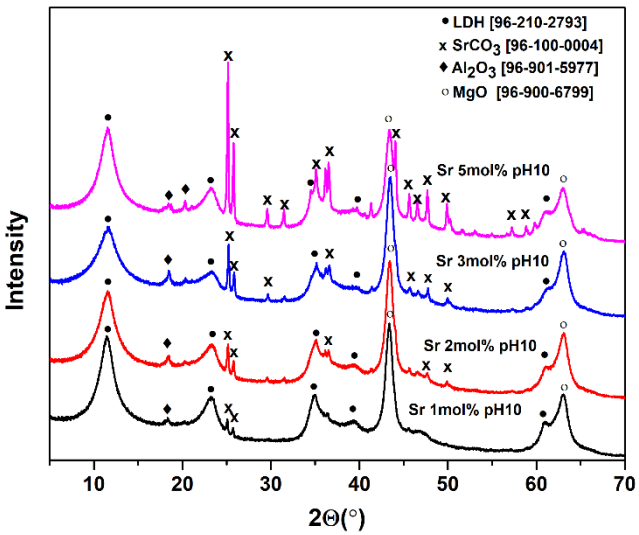

Fig. 10. XRD patterns of the sol-gel derived $Mg_{2-x}Sr_x/Al_1$ LDHs.

The XRD results obtained on barium substitution in $Mg_{2-x}Ba_x/Al_1$ LDHs are very similar to ones discussed above on the formation of $Mg_{2-x}Sr_x/Al_1$ LDHs (**Figs. 11, 12 and 13**). Only about 2% mol of barium could be introduced instead of magnesium to Mg_2Al_1 LDHs synthesized by indirect sol-gel processing.

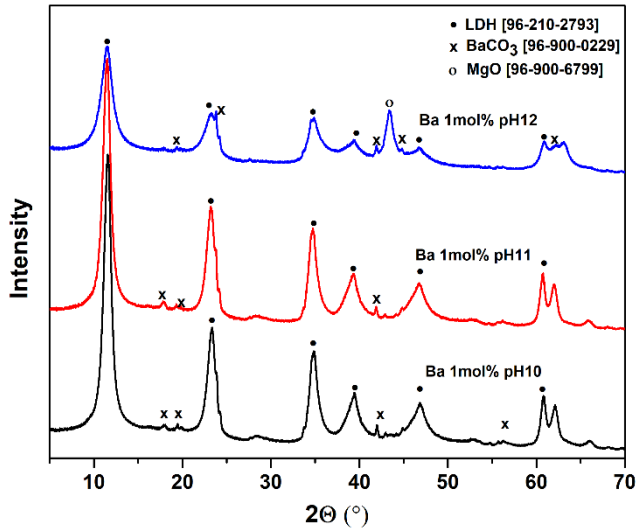

Fig. 11. XRD patterns of sol-gel derived $Mg_{1.98}Ba_{0.02}/Al_1$ LDHs obtained at different pH.

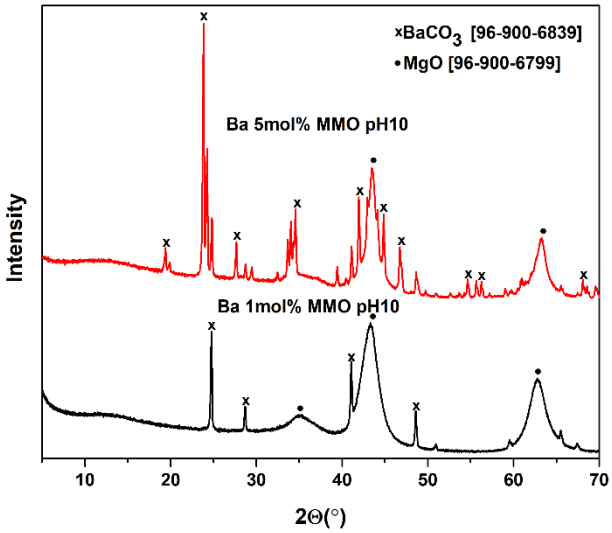

Fig. 12. XRD patterns of mixed-metal oxides (MMO) obtained by heating the $Mg_{2-x}Ba_x/Al_1$ precursor gels at 650 °C.

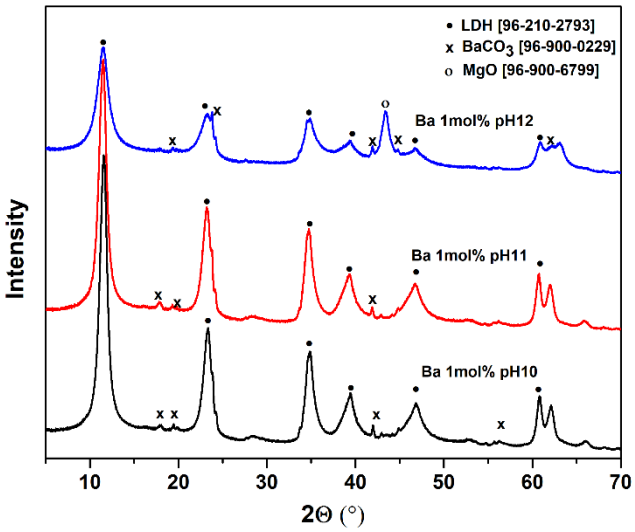

Fig.13. XRD patterns of the sol-gel derived $Mg_{2-x}Ba_x/Al_1$ LDHs.

The interplanar spacings and lattice parameters of purest $Mg_{2-x}M_x/Al_1$ (M = Ca, Sr and Ba) LDH samples synthesized by the sol-gel method are calculated and summarized in **Table 1.** The calculated values of parameter *a* for $Mg_{2-x}Ca_x/Al_1$ are not changing monotonically, however, with an increasing amount of Ca. Parameter *a* is a function of both size and ratio of cations M^{2+} and M^{3+}. In this case, if the relatively larger calcium (ionic radius of Ca^{2+} 1.14 Å) substitutes magnesium (ionic radius of Mg^{2+} 0.86 Å) in the LDH, the cation-cation distance in the brucite-like layers expected to be expanded. As a result of the magnesium-to-calcium substitution, the *a* parameter should grow. However, the parameter *c* determined for $Mg_{2-x}Ca_x/Al_1$ specimens increases almost linearly with an increasing amount of calcium. At least, we can state that about 2-3% mol of magnesium is evidently substituted by calcium in $Mg_{2-x}Ca_x/Al_1$. On the other hand, the calculated lattice parameters of $Mg_{2-x}Sr_x/Al_1$ let us conclude that the introduction of strontium into magnesium sites is problematic. Oppositely, both *a* and *c* parameters for $Mg_{2-x}Ba_x/Al_1$ LDHs increased with an increasing amount of barium in confirming that magnesium

could be replaced even by larger barium (ionic radius of Ba^{2+} 1.49 Å) but probably not by strontium (ionic radius of Sr^{2+} 1.32 Å).

Table 1. The interplanar spacings and lattice parameters of sol-gel derived $Mg_{2-x}M_x/Al_1$ (M= Ca, Sr and Ba) LDHs. Standard deviations in parentheses.

Sample	x, mol %	d (003), Å	d (006), Å	d (110), Å	c, Å	a, Å
$Mg_{2-x}Ca_x/Al_1$	1	7.607(6)	3.802(3)	1.520(1)	22.818(3)	3.040(2)
	2	7.652(4)	3.822(4)	1.522(2)	22.946(5)	3.044(4)
	3	7.692(6)	3.831(3)	1.520(2)	23.031(6)	3.040(4)
	5	7.738(4)	3.857(5)	1.519(3)	23.178(6)	3.039(6)
$Mg_{2-x}Sr_x/Al_1$	1	7.687(5)	3.831(4)	1.517(3)	23.024(7)	3.035(4)
	2	7.664(5)	3.825(3)	1.517(4)	22.974(5)	3.035(5)
$Mg_{2-x}Ba_x/Al_1$	1	7.623(4)	3.801(4)	1.520(3)	22.839(6)	3.039(6)
	2	7.675(7)	3.820(4)	1.521(1)	22.976(5)	3.041(5)

The XRD analysis results confirmed that the substitution of magnesium by alkaline earth metals in the LDHs synthesized using an aqueous sol-gel method highly depends on the nature and concentration of the alkaline earth metal. The ionic crystal radius of metals possibly is not the most important parameter responsible for the level of substitution of magnesium by alkaline earth metals in LDHs. The second parameter could influence the formation of LDH could be a value of the solubility product of metal hydroxides. For example, in the case of $Mg_{2-x}Ca_x/Al_1$ LDH which showed the highest substitutional level, the solubility products are $1.8 \cdot 10^{-11}$ for $Mg(OH)_2$ and $5.5 \cdot 10^{-6}$ for $Ca(OH)_2$. However, the hydroxides of strontium and barium are rather soluble. On the other hand, the solubility product of $SrCO_3$ ($K_{SP} = 4.59 \cdot 10^{-9}$) is slightly lower than the solubility product of $BaCO_3$ ($K_{SP} = 1.13 \cdot 10^{-8}$). This might be the reason that a small amount of barium could be introduced in the $Mg_{2-x}Ba_x/Al_1$ LDH, despite the $Ba(OH)_2$ is sufficiently soluble in water.

Fig. 14 shows the morphological features of calcium-containing MMO obtained by heating the LDHs precursor gels at 650°C and reconstructed $Mg_{2-x}Ca_x/Al_1$ LDHs. The SEM micrographs of Ca containing MMO confirm that the surface of synthesized compounds is composed of large monolithic particles at about 15-20 μm in size. The randomly distributed pores on the chips-coated surface of these monoliths also are seen. The different morphological features could be determined for the reconstructed $Mg_{2-x}Ca_x/Al_1$ LDH samples. The formation of plate-like crystals with a size of 1.5-5 μm in the case of $Mg_{1.98}Ca_{0.02}/Al_1$ was observed. With an increasing amount of calcium in LDH, the sample with more inhomogeneous morphology having larger grains has formed.

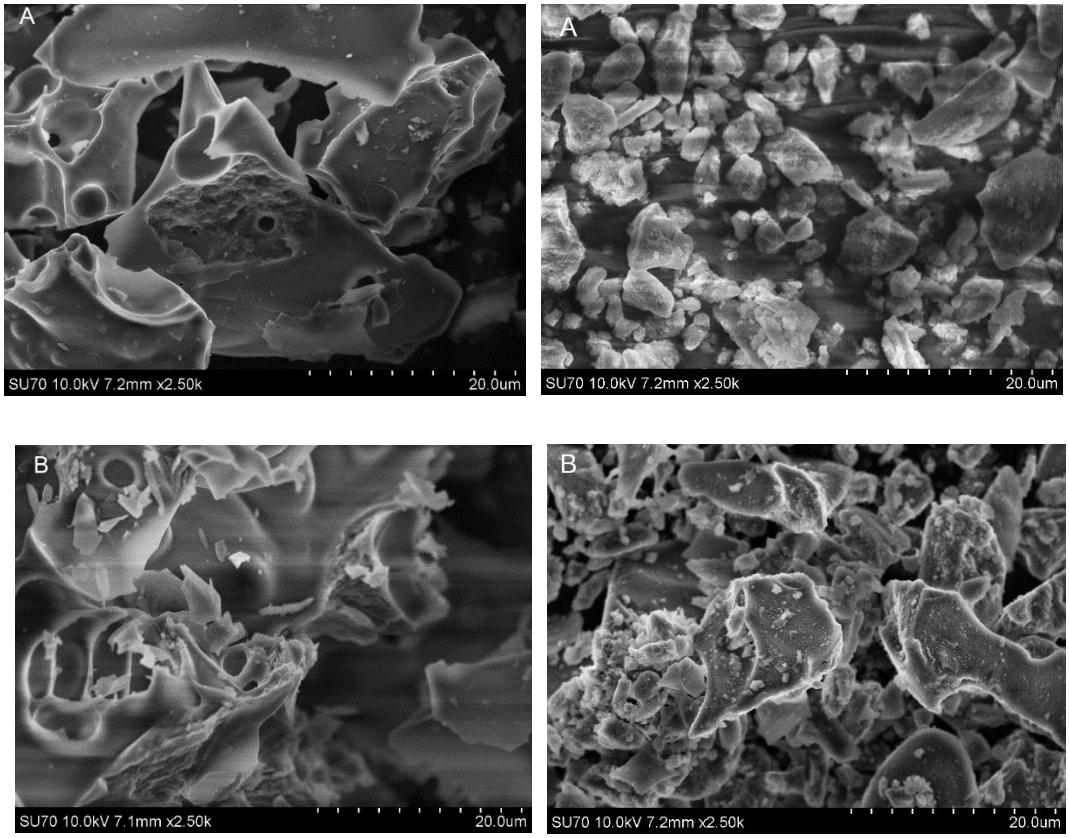

Fig. 14. SEM micrographs of the sol-gel derived $Mg_{2-x}Ca_x/Al_1$ mixed-metal oxides obtained after calcination precursor gels at 650 ^oC (at left) and reconstructed at pH = 10 LDHs (at right). Amount of Ca: 1 mol% (A) and 5 mol% (B).

SEM micrographs of strontium containing MMO and related $Mg_{2-x}Sr_x/Al_1$ LDHs are presented in **Fig. 15.** The surface microstructure of Sr containing MMO is very similar to the Ca containing ones except in the case of the sample with a higher amount of strontium. During the reconstruction of Sr containing MMO, evidently much larger LDHs particles have formed (5-15 μm). The barium containing MMO are composed of the largest (30-40 μm in size) monoliths with less pronounced porous structure (**Fig. 16**). The obtained $Mg_{2-x}Ba_x/Al_1$ LDHs from these MMO show very similar morphology to the $Mg_{2-x}Ca_x/Al_1$ LDHs. The formation of plate-like crystals with a size of 1.5-7.5 μm with well-pronounced connectivity between inner grains occur.

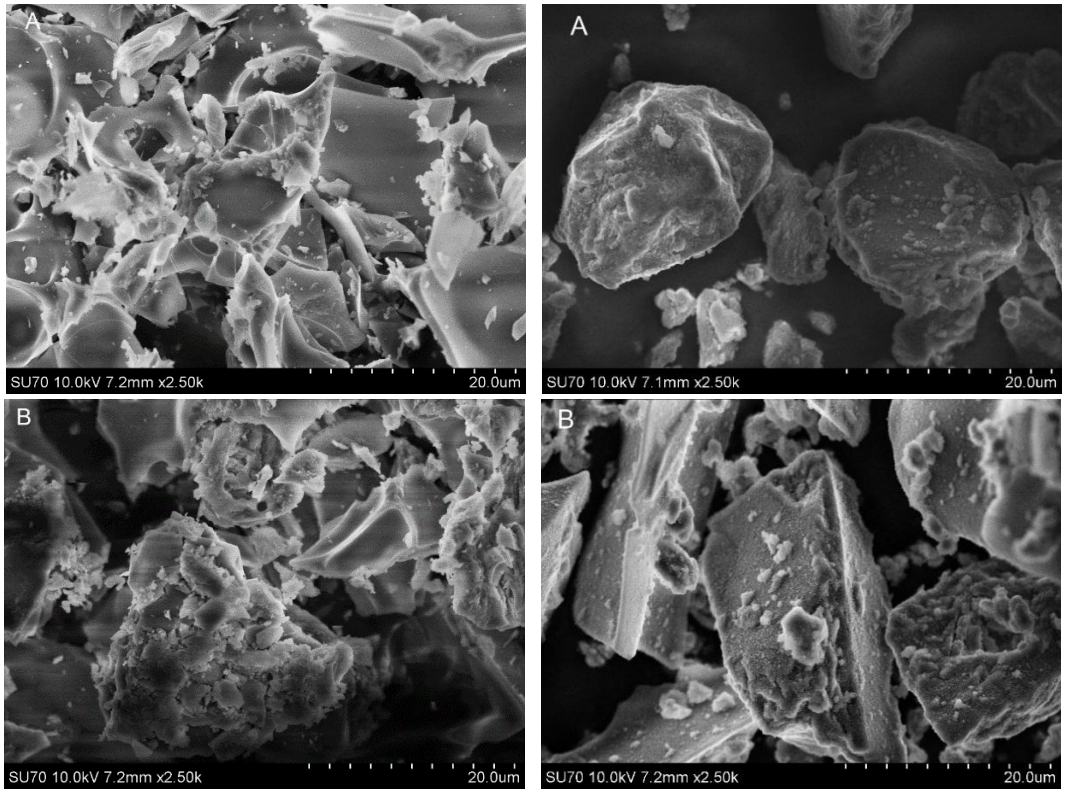

Fig. 15. SEM micrographs of the sol-gel derived $Mg_{2-x}Sr_x/Al_1$ mixed-metal oxides obtained after calcination precursor gels at 650 ºC (at left) and reconstructed at pH = 10 LDHs (at right). Amount of Sr: 1mol% (A) and 5 mol% (B).

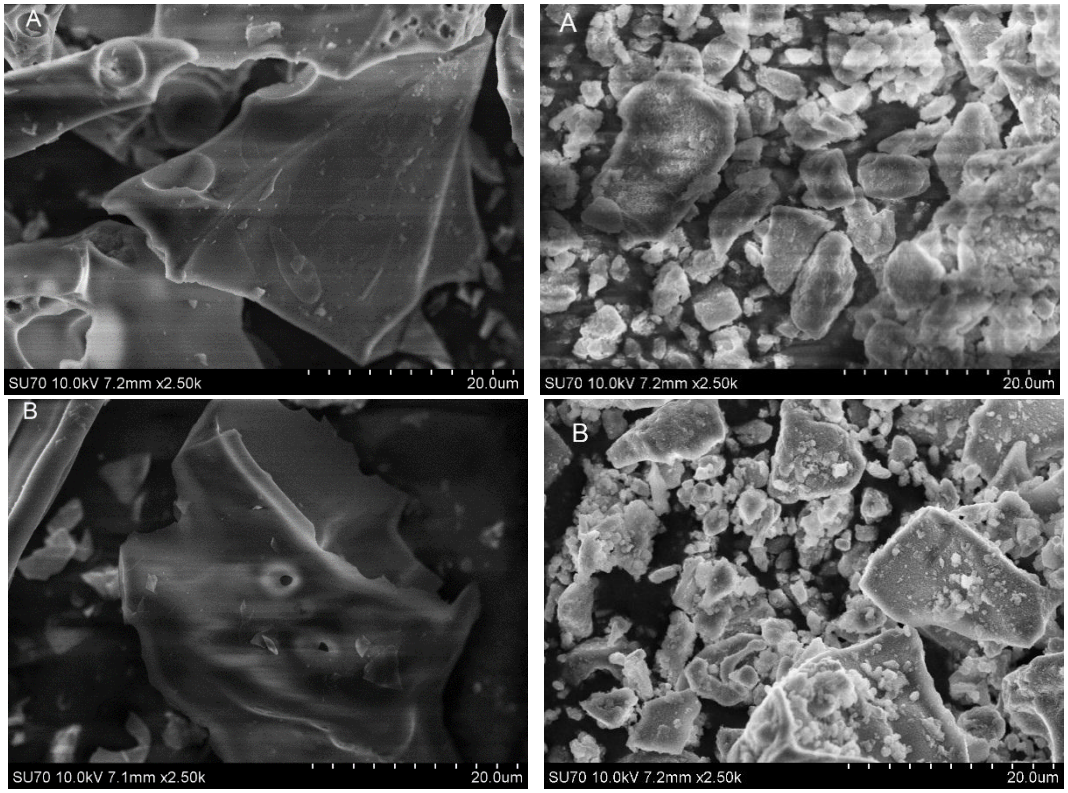

Fig. 16. SEM micrographs of the sol-gel derived $Mg_{2-x}Ba_x/Al_1$ mixed-metal oxides obtained after calcination precursor gels at 650 ºC (at left) and reconstructed at pH = 10 LDHs (at right). Amount of Ba: 1mol% (A) and 3 mol% (B).

The BET results obtained demonstrated that the N_2 adsorption-desorption isotherms of sol-gel synthesized mixed-metal oxides containing Ca, Sr and Ba are very similar except when the

substitutional level of calcium is of 5% mol (**Fig. 17**). The determined N_2 adsorption-desorption isotherms for (1-4% mol) calcium-, strontium-, and barium-containing MMO samples exhibited type IV isotherms with a sharp capillary condensation step at relative pressure, 0.4–0.9. At higher pressure values clearly, the H1 hysteresis loop is seen which indicates the presence of cylindrical mesopores. This type of hysteresis is characteristic for the mesoporous (pore size in the range of 2-50 nm) materials. However, the increase observed at relatively low pressures allows to confirm the type of H4 isotherms and to conclude that the adsorption-desorption isotherms obtained for these MMO samples are qualitatively and quantitatively almost the same. These calcium-, strontium- and barium-containing MMO according to the shape of isotherms could show similar microporosity despite the SEM micrographs showed slightly different results. However, the surface area of MMO sample which contains 5% mol of calcium is different, confirming that for Ca-MMO it depends on the amount of calcium in the specimen. Evidently, the trend of this dependence is not linear. As seen, the isotherm and hysteresis are much pronounced for the MMO with the highest amount of calcium.

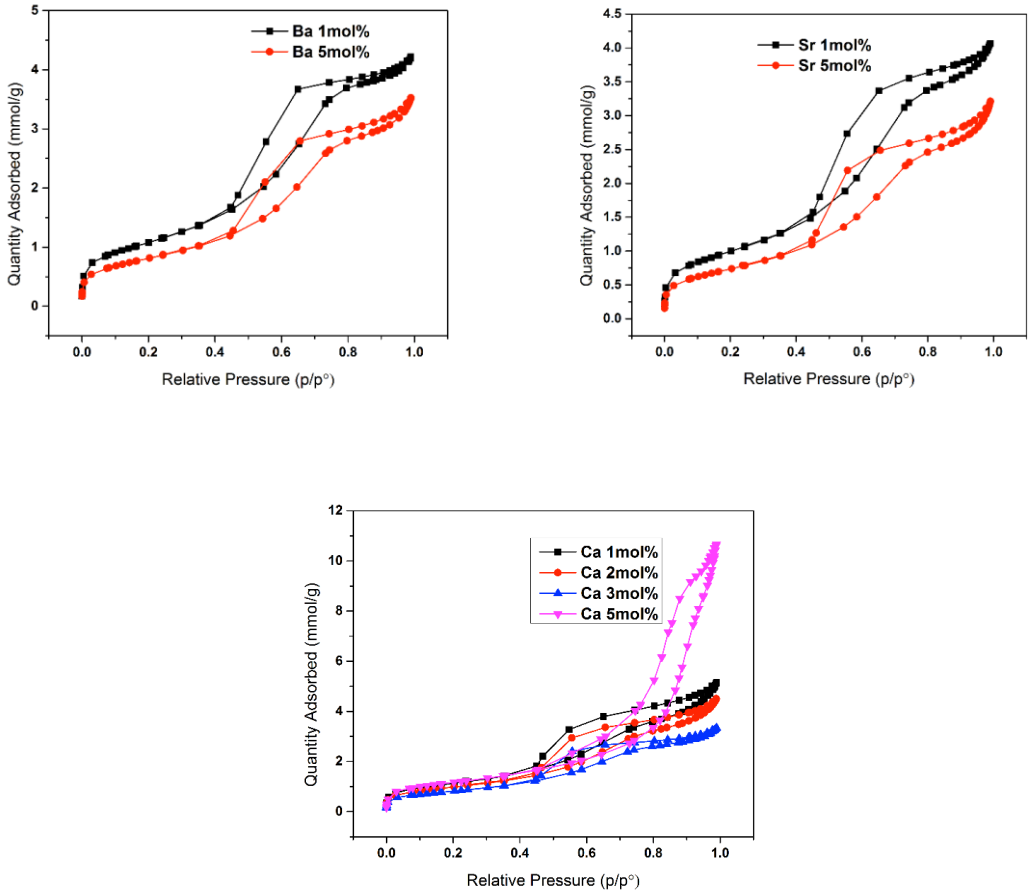

Fig.17. N_2 adsorption-desorption isotherms of MMO containing: Ca (bottom), Sr (upper right) and Ba (upper left).

Fig. 18 shows the pore size distributions obtained by the BJT method for the $Mg_{2-x}M_x/Al_1$ samples. All samples demonstrate narrow pore size distributions (PSD) almost at the microporous level. Moreover, the PSD width slightly depends on the nature of alkaline earth metal in the MMO structure. The average pore diameter in the mesopore region is ~2.5-4.5 nm, ~3-7 nm and ~3-8 nm for the Ca-MMO, Sr-MMO and Ba-MMO samples, respectively. However, the sample with 5% mol of Ca is mesoporous. Some kind of double behaviour is a characteristic feature for this calcium-containing MMO sample. The gain in the volume of mesopores (5-20 nm) is clearly visible. Besides pore diameter, wall thickness probably also increased with an increasing amount of calcium in MMO.

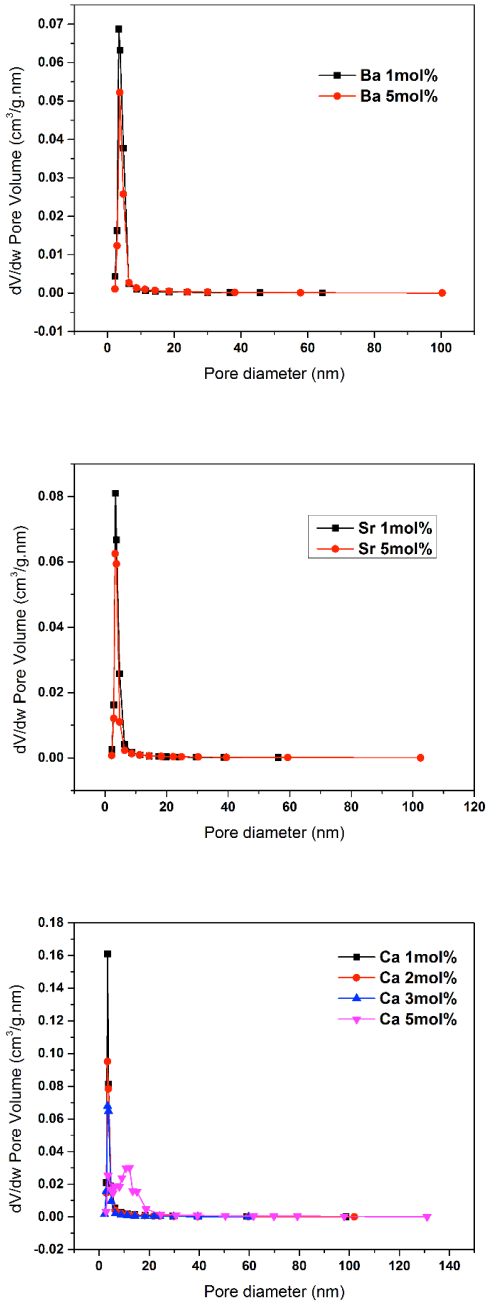

Fig.18. The pore size distribution of MMO containing: Ca (bottom), Sr (middle) and Ba (top).

The results obtained highlighted that the sol-gel preparation method and cation-substitutions can efficiently modify the textural properties of mixed-metal oxides, thus indicating that these MMO could have the potential for the application as catalysts and adsorbents.

3.2 Characterization of modified LDHs.

NO_3^- or Cl^- intercalated LDHs are usually used as the precursors for ion exchange. In this research, the aim was to exchange CO_3^{2-} anions already present in the LDH structure to Cl^- anions with the following intercalation of tartrate and citrate anions into the $Mg_{2-x}M_x/Al_1$-LDH (M = Ca, Sr, Ba, x = 0.02) interlayer space of by anion-exchange method.

The XRD patterns of $Mg_{1.98}Ca_{0.02}/Al_1$-LDH intercalated with anions are presented (**Fig. 19**). The reflections in the XRD patterns of $Mg_{1.98}Ca_{0.02}/Al_1$-LDH-citrate and $Mg_{1.98}Ca_{0.02}/Al_1$-LDH-tartrate synthesized under hydrothermal conditions in a thermobomb are shifted to the smaller 2θ

angle. The shift indicates an increase in the basal spacing values *c* comparing to the respective values for the $Mg_{1.98}Ca_{0.02/}Al_1$-LDH, thus successful intercalation of organic anions. However, the shifts of the $Mg_{1.98}Ca_{0.02/}Al_1$-LDH-citrate and $Mg_{1.98}Ca_{0.02/}Al_1$-LDH-tartrate synthesized under ambient conditions were less pronounced in comparison with the samples obtained under hydrothermal conditions. The XRD results of $Mg_{1.98}Ca_{0.02/}Al_1$-LDH-tartrate synthesized under hydrothermal conditions shows the formation of a side crystalline phase AlO(OH), PDF [00-005-0190].

The calculated lattice parameters of synthesized $Mg_{1,98}Ca_{0,02/}Al_1$-LDH materials and ones intercalated with anions represented in **Table 2.** The lattice parameter a = 2d (110) corresponds to an average cation-cation distance calculated from (110) reflections in brucite-like layers. The parameter c=3/2 [d (003) + 2d (006)] can be affected by the amount of interlayer water and anions, metal molar ratio and the crystallinity of the samples. The results confirm that all anions studied have been successfully intercalated to the $Mg_{1,98}Ca_{0,02/}Al_1$-LDH.

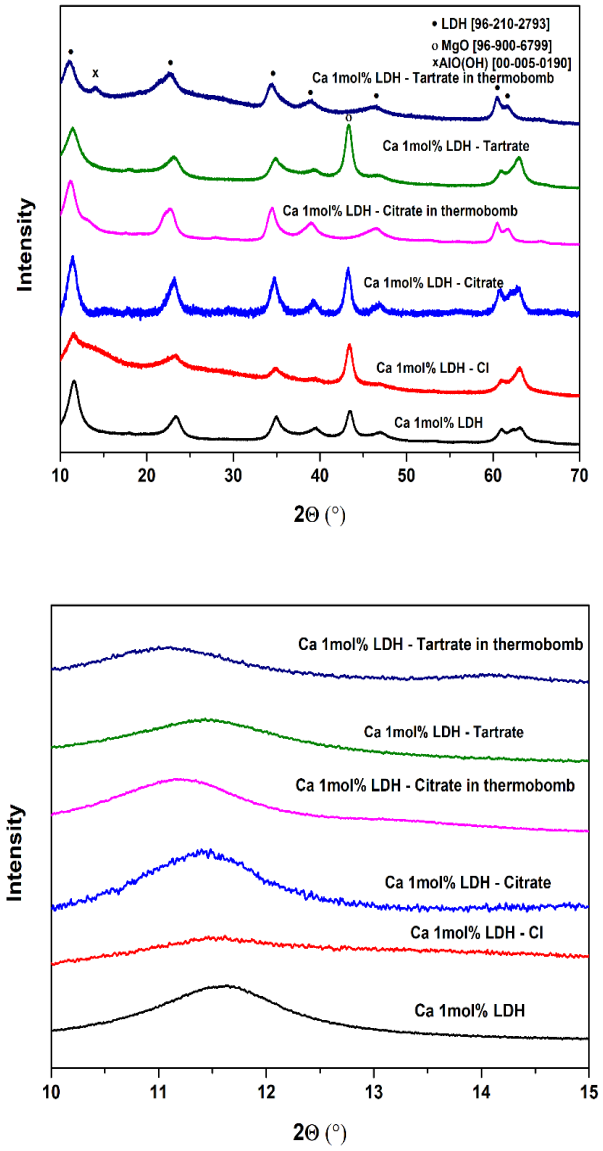

Fig. 19. XRD patterns of $Mg_{2-x}Ca_{x/}Al_1$-LDHs intercalated with anions.

Table 2. Lattice parameters of $Mg_{2-x}Ca_x/Al_1$-LDH with anions intercalated. Standard deviations in parentheses.

Sample	d, (003), Å	d (006), Å	d (110), Å	c, Å	a, Å
$Mg_{2-x}Ca_x/Al_1$-LDH	7.627(2)	3.807(3)	1.518(1)	22.862(7)	3.036(2)
$Mg_{2-x}Ca_x/Al_1$-LDH-Cl	7.685(5)	3.860(4)	1.520(3)	23.109(4)	3.040(6)
$Mg_{2-x}Ca_x/Al_1$-LDH-citrate	7.756(7)	3.864(4)	1.522(7)	23.228(2)	3.045(4)
$Mg_{2-x}Ca_x/Al_1$-LDH-citrate (thermobomb)	7.910(5)	3.927(4)	1.529(1)	23.647(9)	3.058(2)
$Mg_{2-x}Ca_x/Al_1$-LDH-tartrate	7.754(3)	3.860(4)	1.523(6)	23.212(6)	3.047(2)
$Mg_{2-x}Ca_x/Al_1$-LDH-tartrate (thermobomb)	7.925(4)	3.964(0)	1.531(1)	23.780(1)	3.062(1)

FT-IR spectra of $Mg_{2-x}Ca_x/Al_1$-LDH with intercalated citrate and tartrate anions presented in **Fig 20.** The FT-IR spectra for all recorded samples are similar to each other. The broad absorption band observed at around 3300-3500cm^{-1} corresponds to the stretching vibrations of hydroxyl (-OH) groups from the hydroxyl layers and intercalated water molecules. The FT-IR spectra of tartrate and citrate intercalated LDHs show additional absorption bands at 1567 cm^{-1} and 1223 cm^{-1}, which are assigned to the asymmetric and symmetric stretching vibrations of carbon-oxygen bonds of (-COO) group, is more pronounced in the sample synthesized under hydrothermal conditions. The strong absorption band visible at 1350 cm^{-1} is attributed to the asymmetric vibration's modes of ($-CO_3^{2-}$). The absorption bands observed at approximately 650–700 cm^{-1} arises from the metal-oxygen stretch vibrations [91]. Thus, the FT-IR results confirm the intercalation of anion species within the LDH host layers.

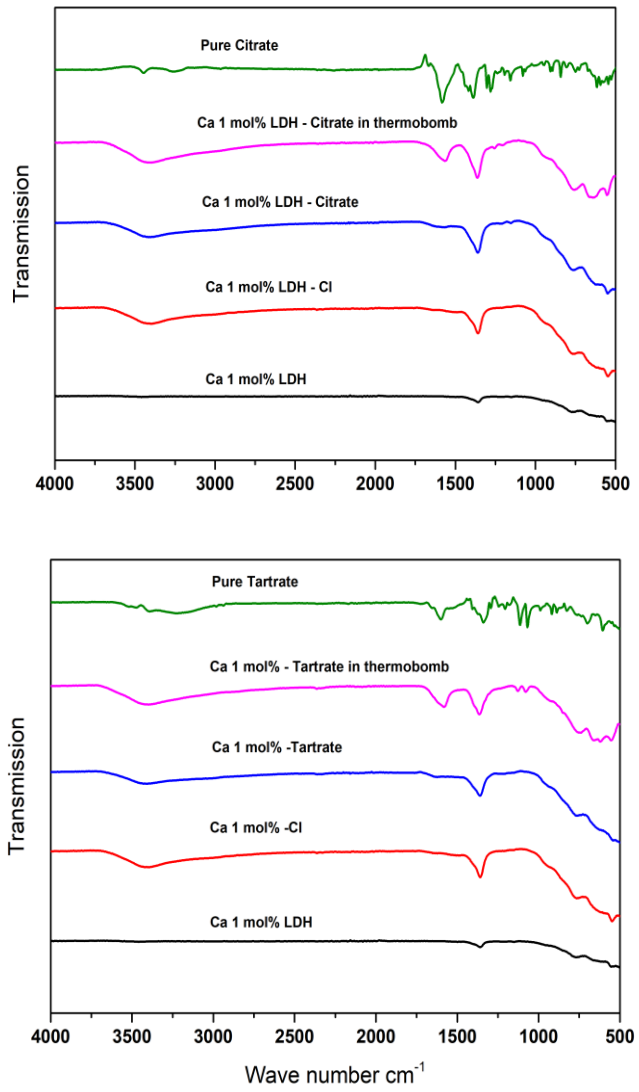

Fig. 20. FT-IR of $Mg_{2-x}Ca_x/Al_1$-LDH with intercalated citrate (top) and tartrate (bottom) anions.

The morphology of the $Mg_{2-x}Ca_x/Al_1$-LDH intercalated with anions is shown in **Fig 21.** The typical microstructure of LDHs is evident from these SEM micrographs. The surface is composed of the agglomerated plate-like particles of around 500 nm in diameter. The plate-shaped morphology characteristic for LDHs remains visible in these intercalated samples, however, its particles became smoother after the intercalation of organic anions.

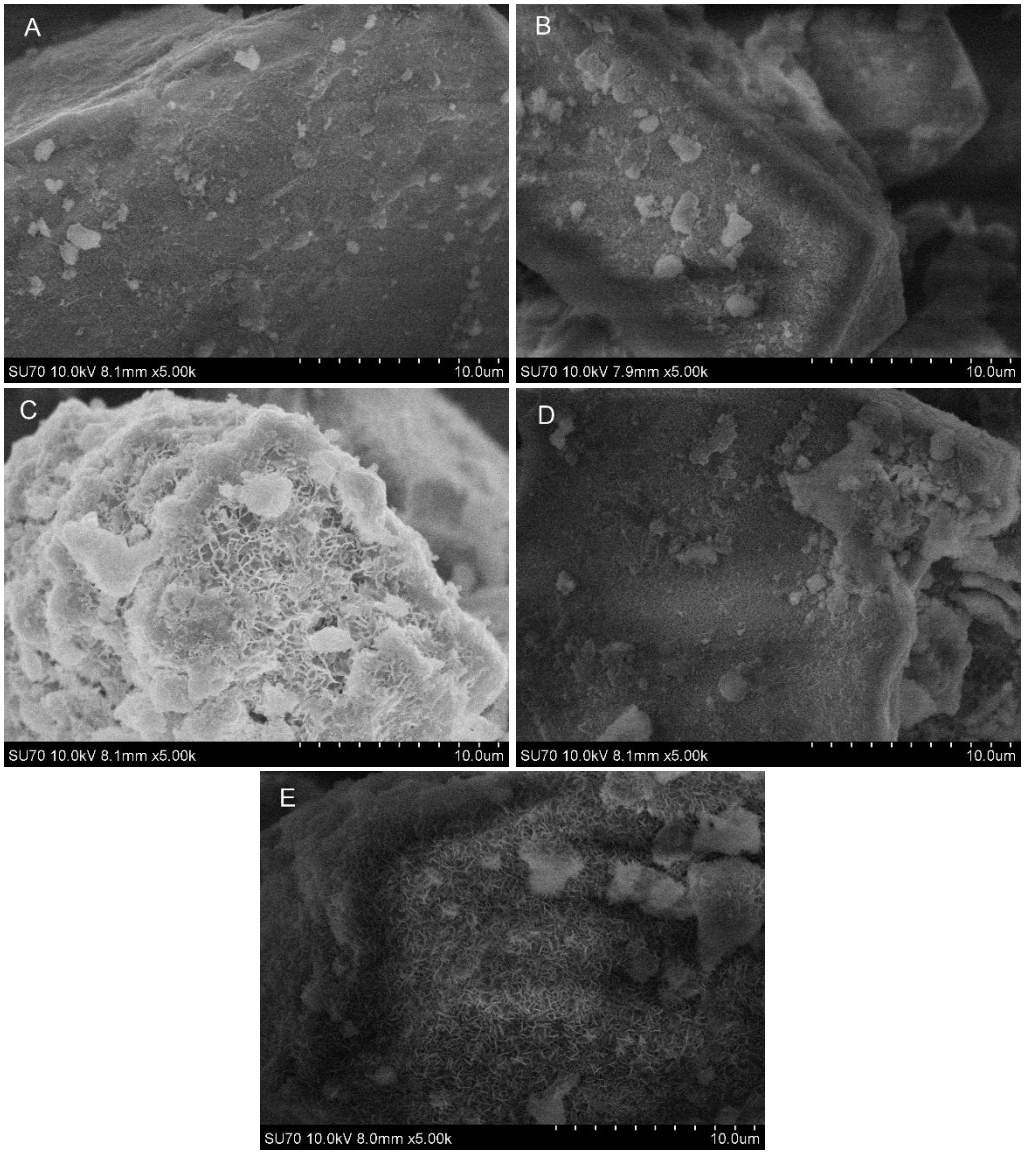

Fig. 21. SEM micrographs of $Mg_{2-x}Ca_x/Al_1$LDH-Cl (A), $Mg_{2-x}Ca_x/Al_1$LDH-citrate (B), $Mg_{2-x}Ca_x/Al_1$LDH-citrate, in thermobomb (C), $Mg_{2-x}Ca_x/Al_1$ LDH-tartrate (D), $Mg_{2-x}Ca_x/Al_1$LDH-tartrate, in thermobomb (E).

The XRD patterns of $Mg_{1.98}Sr_{0.02/}Al_1$-LDH intercalated with anions are presented in **Fig 22.** The results showed the shift of the diffraction peaks of LDH with intercalated anions to smaller 2θ angle values, indicating an increase in the basal spacing values *c* comparing to the respective values for the $Mg_{1.98}Sr_{0.02/}Al_1$-LDH, thus successful intercalation of anions. However, the shifts of the $Mg_{1.98}Sr_{0.02/}Al_1$-LDH-citrate and $Mg_{1.98}Sr_{0.02/}Al_1$-LDH -LDH-tartrate synthesized under ambient conditions were less pronounced in comparison with the samples obtained under hydrothermal conditions. The calculated lattice parameters of synthesized $Mg_{1.98}Sr_{0.02/}Al_1$-LDH materials and ones intercalated with anions represented in **Table 3.** The XRD results of $Mg_{1.98}Sr_{0.02/}Al_1$-LDH-tartrate synthesized under hydrothermal conditions shows the formation of a side crystalline phase AlO(OH), PDF [00-005-0190].

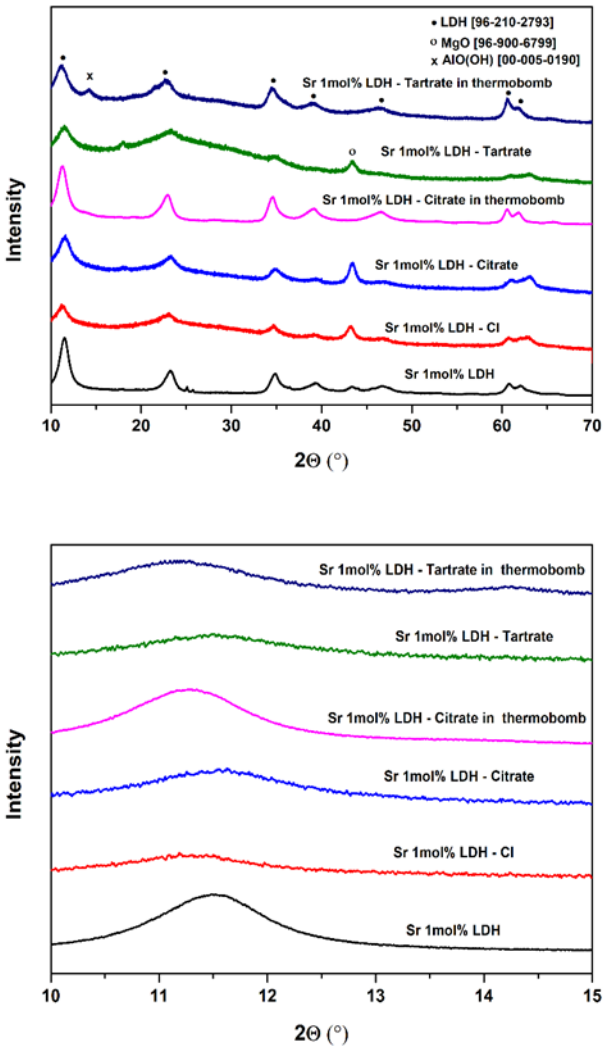

Fig. 22. XRD patterns of $Mg_{2-x}Sr_x/Al_1$-LDHs with intercalated anions.

Table 3. Lattice parameters of $Mg_{2-x}Sr_x/Al_1$-LDH with anions intercalated. Standard deviations in parentheses.

Sample	d, (003), Å	d (006), Å	d (110), Å	c, Å	a, Å
$Mg_{2-x}Sr_x/Al_1$-LDH	7.685(8)	3.825(5)	1.522(7)	23.005(2)	3.045(4)
$Mg_{2-x}Sr_x/Al_1$-LDH-Cl	7.823(8)	3.884(9)	1.524(4)	23.390(4)	3.048(8)
$Mg_{2-x}Sr_x/Al_1$-LDH-citrate	7.691(6)	3.865(4)	1.521(6)	23.133(6)	3.043(2)
$Mg_{2-x}Sr_x/Al_1$-LDH-citrate (thermobomb)	7.817(8)	3.9231()	1.526(0)	23.496(0)	3.052(0)
$Mg_{2-x}Sr_x/Al_1$-LDH-tartrate	7.743(5)	3.868(4)	1.523(5)	23.220(4)	3.047(0)
$Mg_{2-x}Sr_x/Al_1$-LDH-tartrate (thermobomb)	7.896(2)	3.955(7)	1.527(9)	23.711(4)	3.055(8)

FT-IR spectra in the region of 4000-500 cm^{-1} of $Mg_{2-x}Sr_x/Al_1$-LDH with intercalated anions are shown in **Fig 23.** The broad absorption band observed at around 3300-3500 cm^{-1} corresponds to the

stretching vibrations of hydroxyl (-OH) groups from the hydroxyl layers and from intercalated water molecules. The FT-IR spectra of tartrate and citrate intercalated LDHs show additional absorption bands at 1567 cm^{-1} and 1223 cm^{-1}, which are assigned to the asymmetric and symmetric stretching vibrations of carbon-oxygen bonds of (-COO) group, is more pronounced in hydrothermal conditions. The strong absorption band visible at 1350 cm^{-1} is attributed to the asymmetric vibration's modes of ($-CO_3^{2-}$). The absorption bands observed at approximately 650–700 cm^{-1} could be from the metal-oxygen stretch vibrations. FT-IR spectra data confirms that tartrate and citrate anions are intercalated in LDHs.

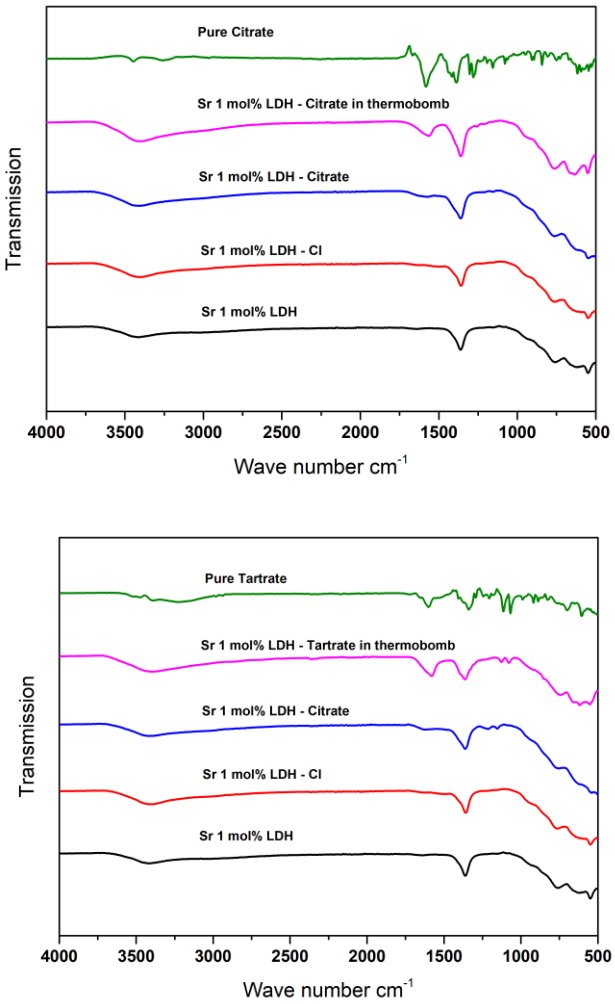

Fig 23. FT-IR of $Mg_{2-x}Sr_x/Al_1$-LDH with intercalated citrate (top) and tartrate (bottom) anions.

SEM micrographs of $Mg_{2-x}Sr_x/Al_1$-LDH with anions intercalated are shown in **Fig. 24.** The typical microstructure of LDHs is evident from these SEM micrographs. The surface is composed of the agglomerated plate-like particles of around 400-500 nm in diameter. The plate-shaped morphology characteristic for LDHs remains visible in these intercalated samples, however, its particles became smoother after the intercalation of organic anions.

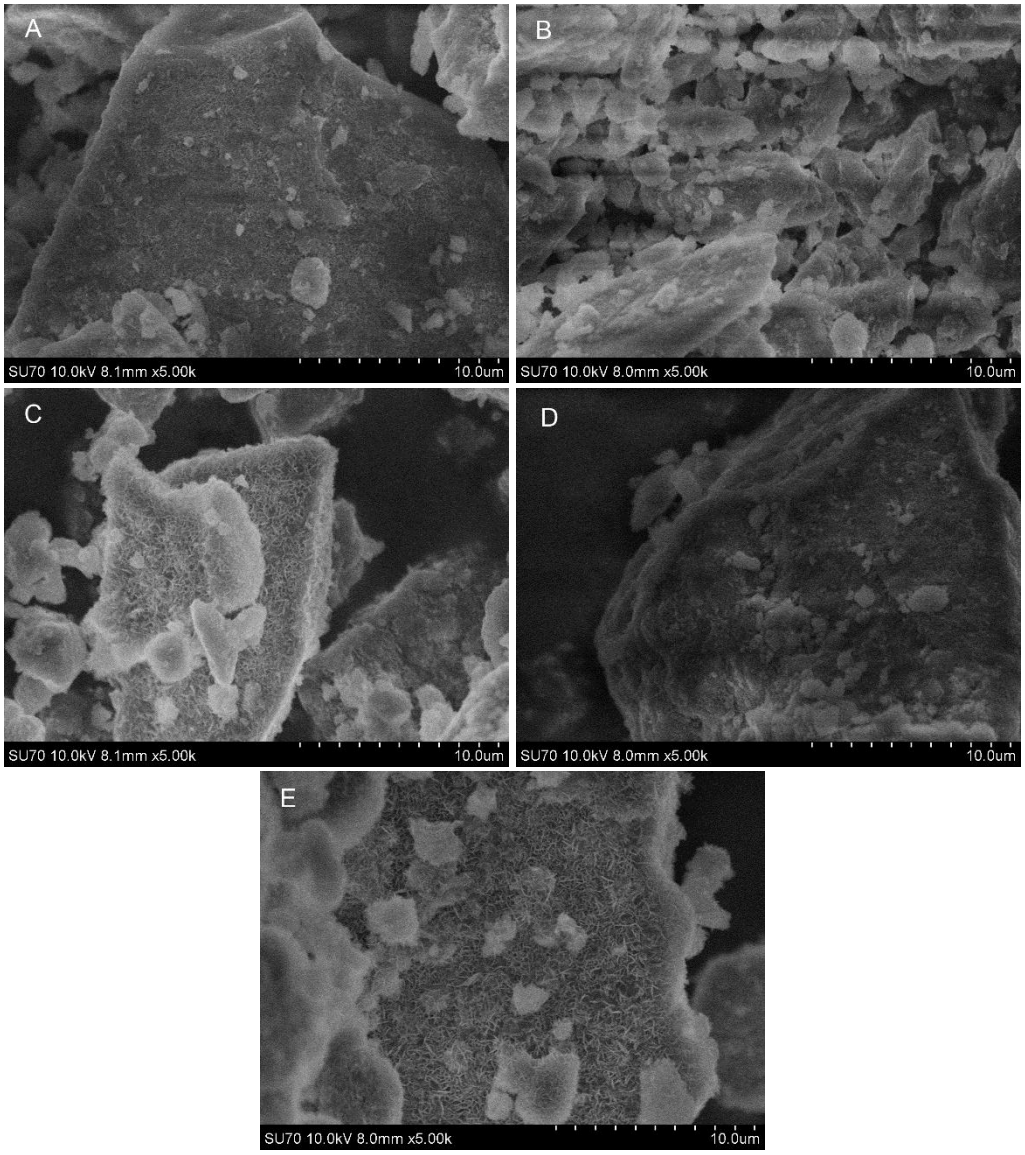

Fig. 24. SEM micrographs of $Mg_{2-x}Sr_x/Al_1$-LDH-Cl (A), $Mg_{2-x}Sr_x/Al_1$-LDH-citrate (B), $Mg_{2-x}Sr_x/Al_1$LDH-citrate, synthesized in thermobomb (C), $Mg_{2-x}Sr_x/Al_1$-LDH-tartrate (D), $Mg_{2-x}Sr_x/Al_1$-LDH-tartrate, in thermobomb (E).

The XRD patterns of $Mg_{1.98}Ba_{0.02/}Al_1$-LDH intercalated with anions are presented in **Fig 25.** The results were similar to the $Mg_{1.98}Ca_{0.02/}Al_1$-LDH and $Mg_{1.98}Sr_{0.02/}Al_1$-LDH samples and showed the shift of the diffraction peaks of $Mg_{1.98}Ba_{0.02/}Al_1$-LDH with intercalated anions to smaller 2θ angle values. The basal spacing values *c* increased comparing to the respective values for $Mg_{1.98}Ba_{0.02/}Al_1$-LDH, indicating successful intercalation of anions. However, the shifts of the $Mg_{1.98}Ba_{0.02/}Al_1$-LDH-citrate and $Mg_{1.98}Ba_{0.02/}Al_1$-LDH-tartrate synthesized under ambient conditions were less pronounced in comparison with the samples obtained under hydrothermal conditions The calculated lattice parameters of synthesized $Mg_{1.98}Ba_{0.02/}Al_1$-LDH materials and ones intercalated with anions represented in **Table 4**. The XRD results of $Mg_{1.98}Ba_{0.02/}Al_1$-LDH-tartrate synthesized under hydrothermal conditions shows the formation of a side crystalline phase AlO(OH), PDF [00-005-0190].

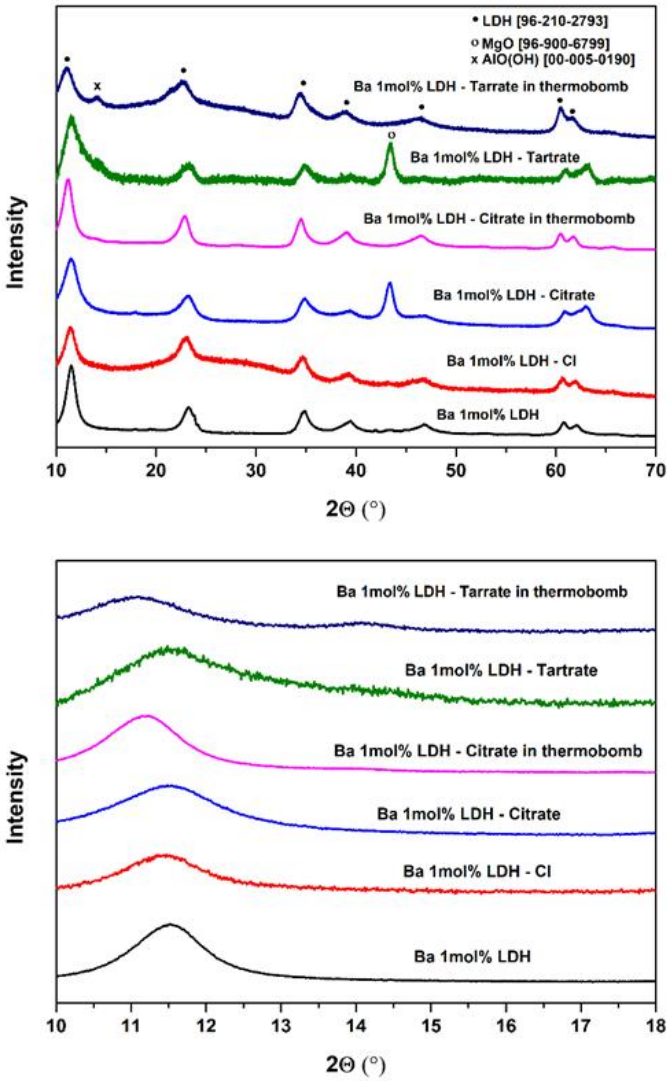

Fig. 25. XRD patterns of $Mg_{2-x}Ba_x/Al_1$-LDHs with intercalated with anions.

Table 4. Lattice parameters of $Mg_{2-}Ba_x/Al_1$-LDH with various anions intercalated. Standard deviations in parentheses.

Sample	d, (003), Å	d (006), Å	d (110), Å	c, Å	a, Å
$Mg_{2-x}Ba_x/Al_1$-LDH	7.667(8)	3.822(7)	1.522(3)	22.969(8)	3.044(6)
$Mg_{2-x}Ba_x/Al_1$-LDH-Cl	7.703(8)	3.865(5)	1.524(3)	23.152(2)	3.048(6)
$Mg_{2-x}Ba_x/Al_1$-LDH-citrate	7.687(7)	3.858(3)	1.522(4)	23.106(4)	3.044(8)
$Mg_{2-x}Ba_x/Al_1$-LDH-citrate (thermobomb)	7.897(5)	3.906(8)	1.531(3)	23.566(6)	3.062(6)
$Mg_{2-x}Ba_x/Al_1$-LDH-tartrate	7.734(4)	3.838(2)	1.523(3)	23.116(2)	3.046(6)
$Mg_{2-x}Ba_x/Al_1$-LDH-tartrate (thermobomb)	7.889(0)	3.877(5)	1.522(8)	23.466(0)	3.045(6)

FT-IR spectra of $Mg_{2-x}Ba_x/Al_1$-LDH-anion are similar to the previous samples and independent of the nature of substituted metal (**Fig 26.**). The broad absorption band observed at around 3300-3500cm^{-1} corresponds to the stretching vibrations of hydroxyl (-OH) groups from the hydroxyl layers and from intercalated water molecules. The FT-IR spectra of tartrate and citrate intercalated LDHs

show additional absorption bands at 1567 cm^{-1} and 1223 cm^{-1}, which are assigned to the asymmetric and symmetric stretching vibrations of carbon-oxygen bonds of (-COO) group, is more pronounced hydrothermal conditions. The strong absorption band visible at 1350 cm^{-1} is attributed to the asymmetric vibration's modes of ($-CO_3^{2-}$). The absorption bands observed at approximately 650–700 cm^{-1} could be from the metal-oxygen stretch vibrations. Hence, FT-IR spectroscopy results confirm the high reproducibility of sol-gel processing used in this study for the preparation of mixed-metal LDH with intercalated anions.

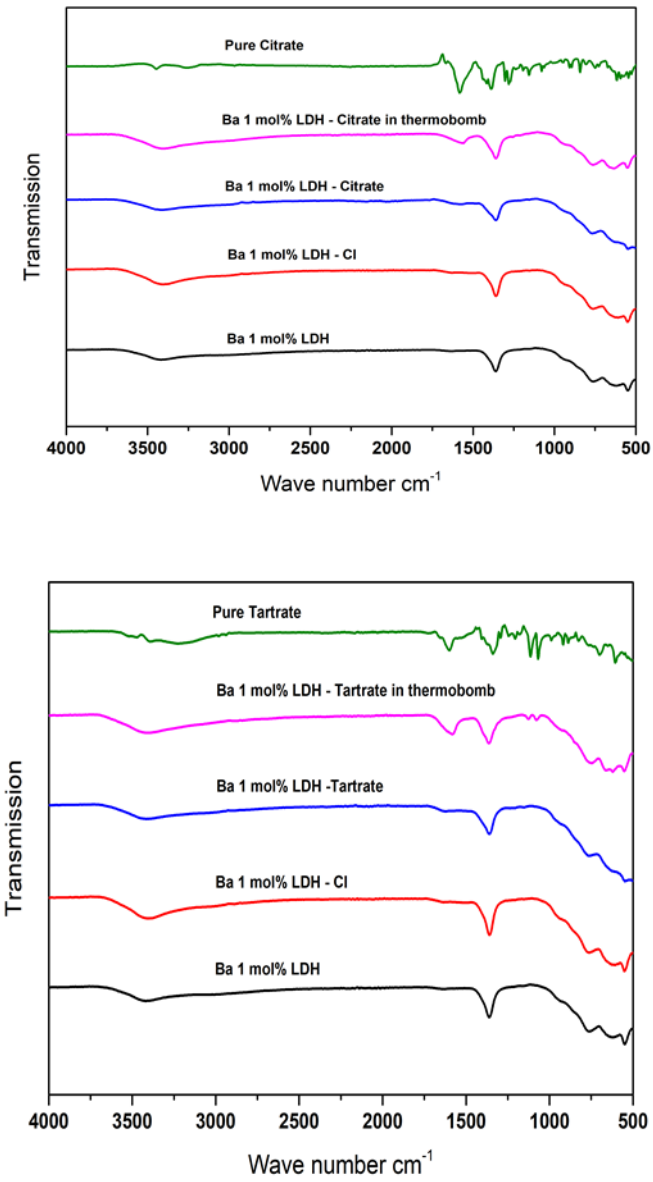

Fig. 26. FT-IR of $Mg_{2-x}Ba_x/Al_1$-LDH with intercalated citrate (top) and tartrate (bottom) anions.

SEM micrographs of $Mg_{2-x}Ba_x/Al_1$-LDH with anions intercalated are shown in **Fig 27.** The typical microstructure of LDHs is evident from these SEM micrographs. The surface is composed of the agglomerated plate-like particles of around 500 nm in diameter. The plate-shaped morphology characteristic for LDHs remains visible in these intercalated samples, however, its particles became smoother after the intercalation of organic anions.

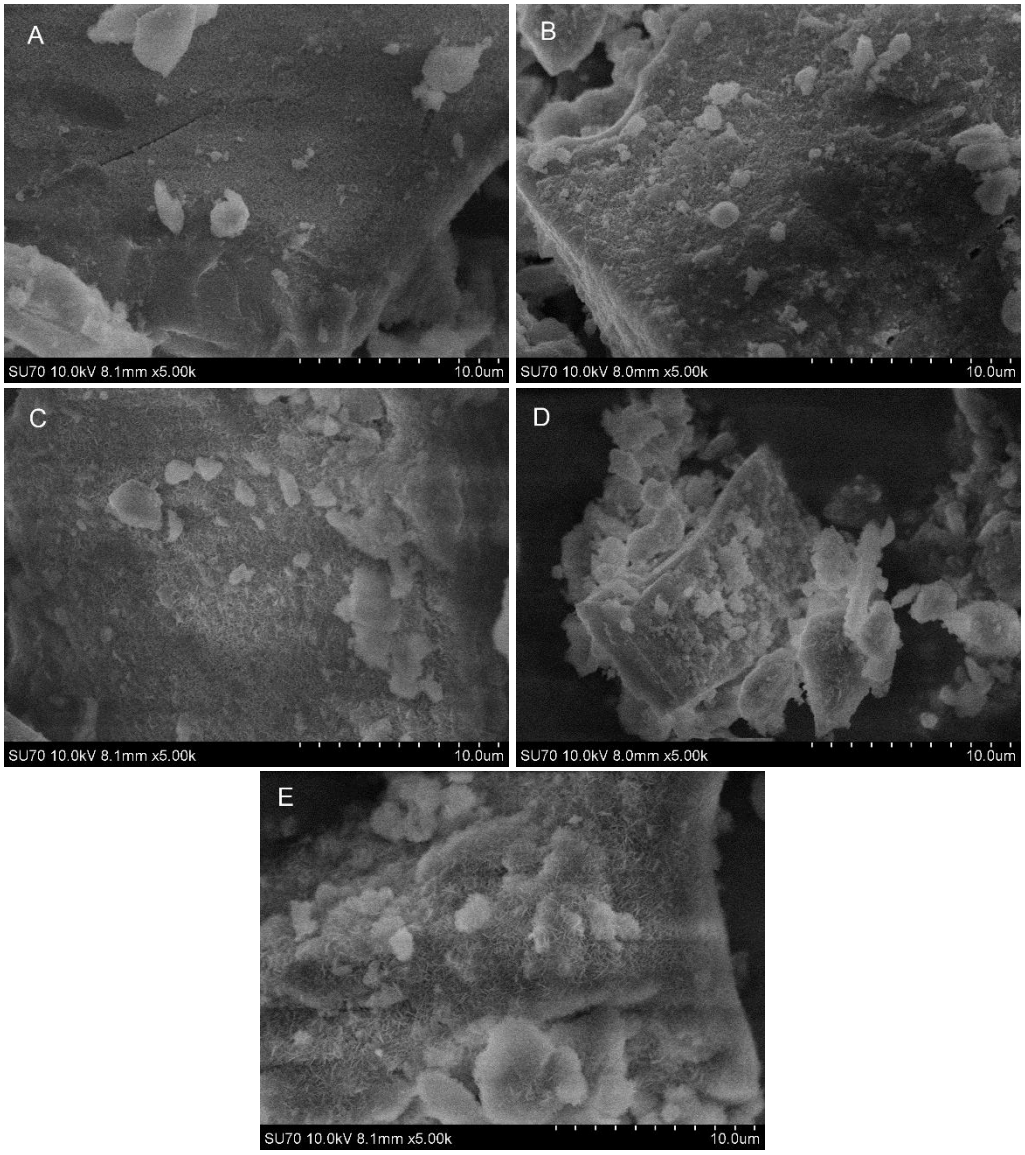

Fig. 27. SEM micrographs of $Mg_{2-x}Ba_x/Al_1$-LDH-Cl (A), $Mg_{2-x}Ba_x/Al_1$-LDH-citrate (B), $Mg_{2-x}Ba_x/Al_1$-LDH-citrate, in thermobomb (C), $Mg_{2-x}Ba_x/Al_1$-LDH-tartrate(D), $Mg_{2-x}Ba_x/Al_1$-LDH-tartrate, in thermobomb (E).

The XRD patterns of magnesium unsubstituted Mg_2Al_1-LDH samples modified with anions are presented in **Fig 28.** The calculated lattice parameters of synthesized Mg_2Al_1-LDH materials and ones intercalated with anions represented in **Table 5.** The lattice parameter *c* increased, thus indicating an increase of the basal spacing and anion exchange of anions into the LDH host structure. The results showed the shift of the diffraction peaks of Mg_2Al_1-LDH with intercalated anions to smaller 2θ angle values. The basal spacing values *c* increased comparing to the respective values for Mg_2Al_1-LDH, indicating successful intercalation of anions. However, the shifts of the Mg_2Al_1-LDH-citrate and Mg_2Al_1-LDH-tartrate synthesized under ambient conditions were less pronounced in comparison with the samples obtained under hydrothermal conditions. The XRD results of Mg_2Al_1-LDH-tartrate synthesized under hydrothermal conditions shows the formation of a side crystalline phase AlO(OH), PDF [00-005-0190].

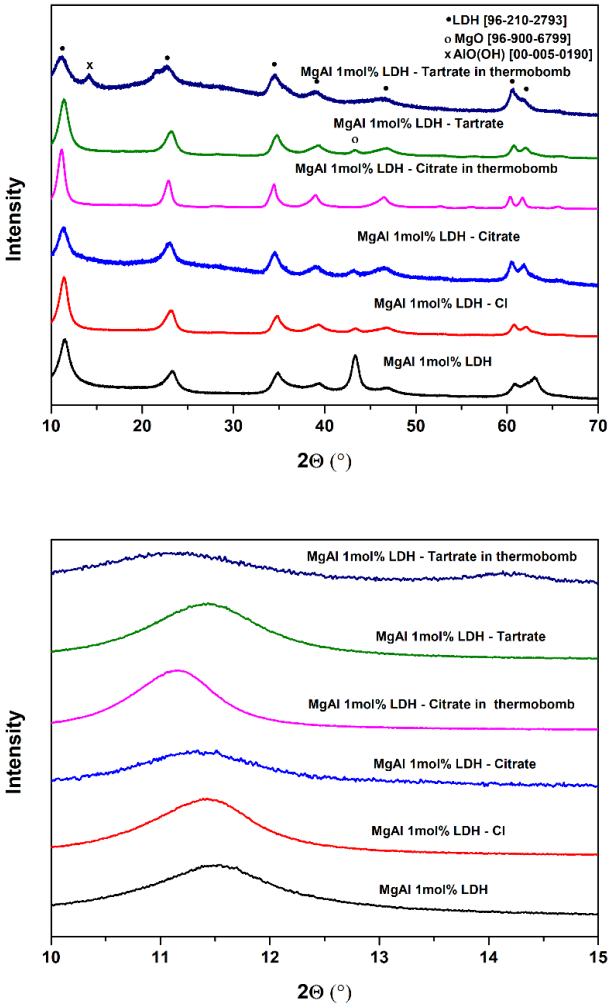

Fig. 28. XRD patterns of Mg_2Al_1-LDHs with intercalated with anions.

Table 5. Lattice parameters of Mg_2/Al_1-LDH with various anions intercalated. Standard deviations in parentheses.

Sample	d, (003), Å	d (006), Å	d (110), Å	c, Å	a, Å
Mg_2/Al_1-LDH	7.682(8)	3.817(2)	1.519(8)	22.975(8)	3.039(6)
Mg_2/Al_1-LDH-Cl	7.730(4)	3.838(2)	1.523(0)	23.110(2)	3.046(0)
Mg_2/Al_1-LDH-citrate	7.778(6)	3.858(2)	1.527(4)	23.242(5)	3.054(8)
Mg_2/Al_1-LDH-citrate (thermobomb)	7.981(7)	3.832(0)	1.577(4)	23.468(5)	3.154(8)
Mg_2/Al_1-LDH-tartrate	7.734(4)	3.838(2)	1.523(3)	23.116(2)	3.046(6)
Mg_2/Al_1-LDH-tartrate (thermobomb)	8.020(1)	3.915(6)	1.532(0)	23.776(9)	3.064(0)

FT-IR spectra of Mg_2/Al_1-LDH with intercalated anions are shown in **Fig. 29.** The broad absorption band observed at around 3300-3500cm^{-1} corresponds to the stretching vibrations of hydroxyl (-OH) groups from the hydroxyl layers and from intercalated water molecules. The FT-IR spectra of tartrate and citrate intercalated LDHs show additional absorption bands at 1567 cm^{-1} and 1223 cm^{-1}, which are assigned to the asymmetric and symmetric stretching vibrations of carbon-oxygen bonds of (-COO) group, is more pronounced in hydrothermal conditions. The strong absorption band visible at 1350 cm^{-1} is attributed to the asymmetric vibration's modes of ($-CO_3^{2-}$).

The absorption bands observed at approximately 650–700 cm^{-1} could be from the metal-oxygen stretch vibrations.

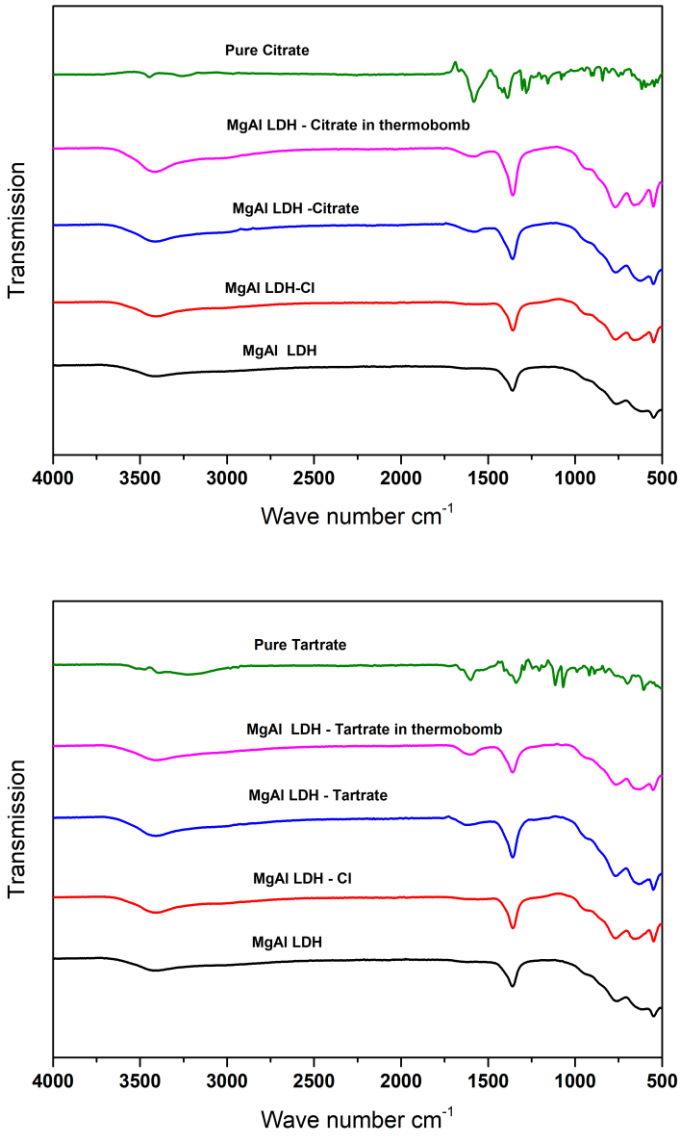

Fig. 29. FT-IR of Mg_2/Al_1-LDH with intercalated citrate (top) and tartrate (bottom) anions.

The morphology of Mg_2/Al_1-LDH with anions intercalated is shown in **Fig 30.** The typical microstructure of LDHs is evident from these SEM micrographs. The surface is composed of the agglomerated plate-like particles of around 300 nm in diameter.

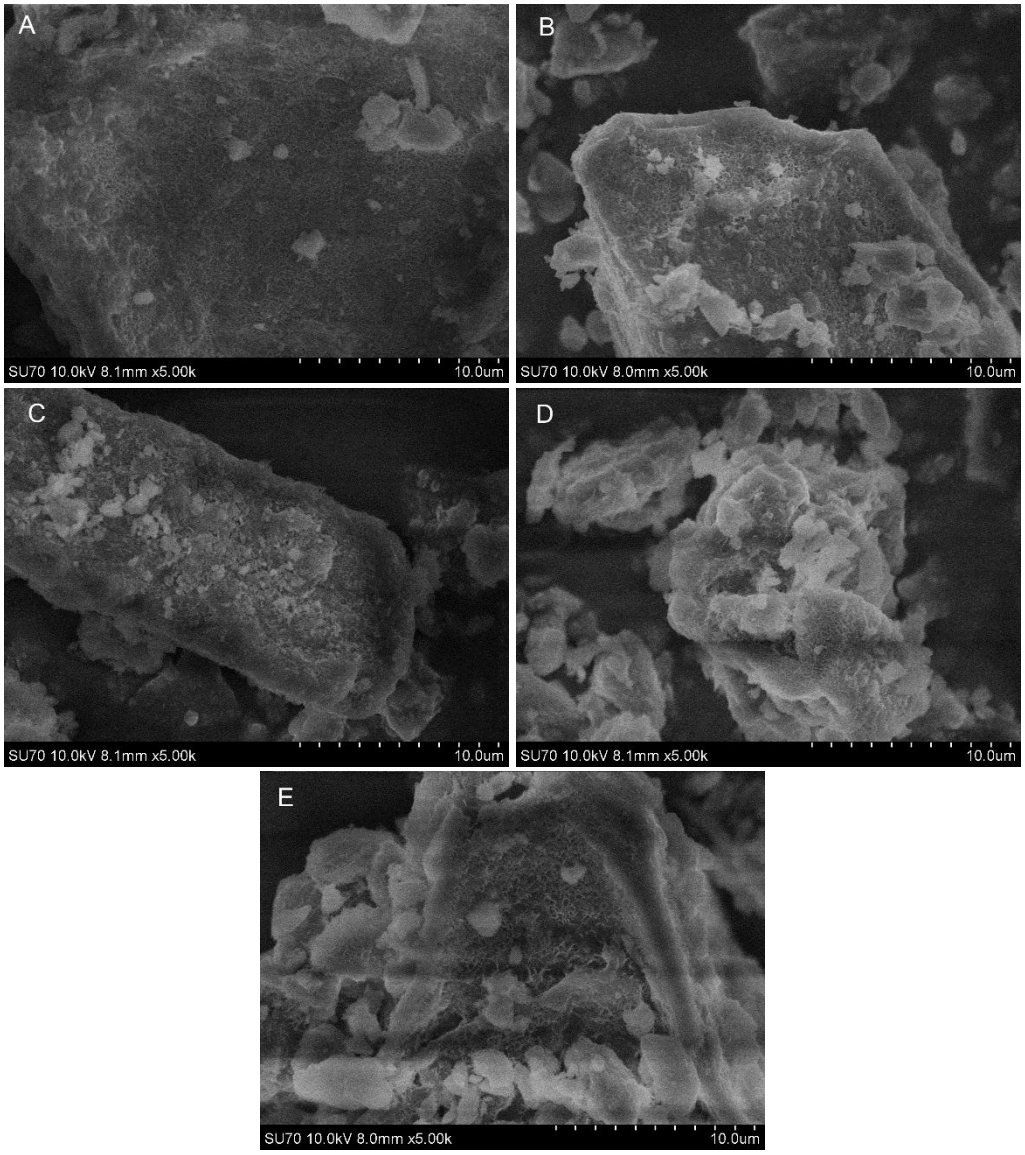

Fig. 30. SEM micrographs of Mg_2/Al_1-LDH-Cl (A), Mg_2/Al_1-LDH-citrate (B), Mg_2/Al_1-LDH-citrate, in thermobomb (C), Mg_2/Al_1-LDH-tartrate (D), Mg_2/Al_1-LDH-tartrate, in thermobomb (E).

The obtained results confirm the intercalation of anions into the $Mg_{2-x}M_x/Al_1$-LDHs hosts.

CONCLUSIONS

1. $Mg_{2-x}M_x/Al_1$ (M = Ca, Sr, Ba) layered double hydroxides and related MMO were obtained by sol-gel synthesis approach. Different amounts of Ca, Sr, Ba were introduced into the sol-gel derived LDHs without destroying the layered structure.

2. The XRD analysis results of synthesized mixed-metal LDHs showed an increase of the lattice parameter *a*, indicating substitution of magnesium by alkaline earth metals. The substitution of metal cations of LDHs depends on the nature and concentration of the introduced alkaline earth metal.

3. Ca, Sr and Ba containing MMO were composed of large monolithic particles with the size of about 15-20 μm, 5-15 μm and 30-40 μm, respectively. The different morphological features were determined for the reconstructed $Mg_{2-x}Ca_x/Al_1$ LDH samples. The formation of plate-like crystals with the size of 1.5-7.5 μm was observed.

4. The average pore diameter in the mesopore region was ~2.5-4.5 nm, ~3-7 nm and ~3-8 nm for the Ca-MMO, Sr-MMO and Ba-MMO samples, respectively.

5. Inorganic chloride anions have been exchanged and intercalated into the $Mg_{2-x}M_x/Al_1$-LDHs (M = Ca, Sr, Ba) hosts by anion exchange method. Based on XRD analysis results lattice parameter *c* has increased, confirming the intercalation of the desired anions into layered double hydroxides.

6. Chloride intercalated LDHs were used for further exchange and intercalation of tartrate and citrate anions into the $Mg_{2-x}M_x/Al_1$-LDHs (M = Ca, Sr, Ba) at different conditions. The XRD and FTIR results supported successful intercalation of desired anions into the structure of LDHs. Intercalation was more pronounced under hydrothermal conditions. SEM micrographs of intercalated samples showed the characteristic plate-like particles of 300 – 500 nm in diameter for $Mg_{2-x}M_x/Al_1$-LDHs (M = Ca, Sr, Ba).

REFERENCES

[1] C. Prasad, H. Tang, Q.Q. Liu, S. Zulfiqar, S. Shah, I. Bahadur, An overview of semiconductors/layered double hydroxides composites: Properties, synthesis, photocatalytic and photoelectrochemical applications, J. Mol. Liq. 289 (2019). https://doi.org/10.1016/j.molliq.2019.111114.

[2] J. Fahel, S. Kim, P. Durand, E. André, C. Carteret, layered double hydroxides for organic pollutants, (2016) 8224–8235. https://doi.org/10.1039/c6dt00441e.

[3] I. Szilagyi, Layered double hydroxide-based nanomaterials-from fundamentals to applications, Nanomaterials. 9 (2019) 10–12. https://doi.org/10.3390/nano9081174.

[4] D.G. Evans, R.C.T. Slade, Structural aspects of layered double hydroxides, Struct. Bond. 119 (2005) 1–87. https://doi.org/10.1007/430_005.

[5] R. Allmann, The crystal structure of pyroaurite, Acta Crystallogr. Sect. B Struct. Crystallogr. Cryst. Chem. 24 (1968) 972–977. https://doi.org/10.1107/s0567740868003511.

[6] H.F.W. Taylor, Segregation and cation-ordering in sjögrenite and pyroaurite, Mineral. Mag. 37 (1969) 338–342. https://doi.org/10.1180/minmag.1969.037.287.04.

[7] G. Mishra, B. Dash, S. Pandey, Layered double hydroxides: A brief review from fundamentals to application as evolving biomaterials, Appl. Clay Sci. 153 (2018) 172–186. https://doi.org/10.1016/j.clay.2017.12.021.

[8] A.I. Khan, D. O'Hare, Intercalation chemistry of layered double hydroxides: Recent developments and applications, J. Mater. Chem. 12 (2002) 3191–3198. https://doi.org/10.1039/b204076j.

[9] K. Klemkaite, A. Khinsky, A. Kareiva, Reconstitution effect of Mg/Ni/Al layered double hydroxide, Mater. Lett. 65 (2011) 388–391. https://doi.org/10.1016/j.matlet.2010.10.039.

[10] P.X. Zhi, Q.L. Guo, Hydrothermal synthesis of layered double hydroxides (LDHs) from mixed MgO and Al2O3: LDH formation mechanism, Chem. Mater. 17 (2005) 1055–1062. https://doi.org/10.1021/cm048085g.

[11] F. Prinetto, G. Ghiotti, P. Graffin, D. Tichit, Synthesis and characterization of sol-gel Mg/Al and Ni/Al layered double hydroxides and comparison with co-precipitated samples, Microporous Mesoporous Mater. 39 (2000) 229–247. https://doi.org/10.1016/S1387-1811(00)00197-9.

[12] D. Sokol, M. Ivanov, A.N. Salak, R. Grigalaitis, J. Banys, A. Kareiva, Dielectric properties of Bi-substituted LDHs synthesized by co-precipitation and sol-gel methods, Mater. Sci. Pol. 37 (2019) 190–195. https://doi.org/10.2478/msp-2019-0035.

[13] A. Smalenskaite, M.M. Kaba, I. Grigoraviciute-Puroniene, L. Mikoliunaite, A. Zarkov, R. Ramanauskas, I.A. Morkan, A. Kareiva, Sol-gel synthesis and characterization of coatings of Mg-Al layered double hydroxides, Materials (Basel). 12 (2019) 27–29. https://doi.org/10.3390/ma12223738.

[14] K. Takehira, T. Shishido, Preparation of supported metal catalysts starting from hydrotalcites as the precursors and their improvements by adopting "memory effect," Catal. Surv. from Asia. 11 (2007) 1–30. https://doi.org/10.1007/s10563-007-9016-2.

[15] J.S. Valente, E. Lima, J.A. Toledo-Antonio, M.A. Cortes-Jacome, L. Lartundo-Rojas, R. Montiel, J. Prince, Comprehending the thermal decomposition and reconstruction process of sol-gel MgAl layered double hydroxides, J. Phys. Chem. C. 114 (2010) 2089–2099. https://doi.org/10.1021/jp910538r.

[16] M. Laipan, J. Yu, R. Zhu, J. Zhu, A.T. Smith, H. He, D. O'Hare, L. Sun, Functionalized layered double hydroxides for innovative applications, Mater. Horizons. 7 (2020) 715–745. https://doi.org/10.1039/c9mh01494b.

[17] T.H. Kim, W.J. Lee, J.Y. Lee, S.M. Paek, J.M. Oh, Isomorphous substitution of divalent metal ions in layered double hydroxides through a soft chemical hydrothermal reaction, Dalt. Trans. 43 (2014) 10430–10437. https://doi.org/10.1039/c4dt00373j.

[18] M. Gong, Y. Li, H. Zhang, B. Zhang, W. Zhou, J. Feng, H. Wang, Y. Liang, Z. Fan, J. Liu, H. Dai, Ultrafast high-capacity NiZn battery with NiAlCo-layered double hydroxide, Energy Environ. Sci. 7 (2014) 2025–2032. https://doi.org/10.1039/c4ee00317a.

[19] C. Prasad, H. Tang, Q.Q. Liu, S. Zulfiqar, S. Shah, I. Bahadur, An overview of semiconductors/layered double hydroxides composites: Properties, synthesis, photocatalytic and photoelectrochemical applications, J. Mol. Liq. 289 (2019). https://doi.org/10.1016/j.molliq.2019.111114.
[20] Z.P. Xu, G.Q.M. Lu, Layered double hydroxide nanomaterials as potential cellular drug delivery agents *, 78 (2006) 1771–1779. https://doi.org/10.1351/pac200678091771.
[21] S. Tang, H.K. Lee, Application of dissolvable layered double hydroxides as sorbent in dispersive solid-phase extraction and extraction by co-precipitation for the determination of aromatic acid anions, Anal. Chem. 85 (2013) 7426–7433. https://doi.org/10.1021/ac4013573.
[22] P. Gu, S. Zhang, X. Li, X. Wang, T. Wen, R. Jehan, A. Alsaedi, T. Hayat, X. Wang, Recent advances in layered double hydroxide-based nanomaterials for the removal of radionuclides from aqueous solution, Environ. Pollut. 240 (2018) 493–505. https://doi.org/10.1016/j.envpol.2018.04.136.
[23] H. Pfeiffer, L. Martínez-dlCruz, E. Lima, J. Flores, M. A. Vera, J. S. Valente, Influence of Mg/Al Ratio on the Thermokinetic Rehydration of Calcined Mg−Al Layered Double Hydroxides, J. Phys. Chem. C. 114 (2010) 8485–8492. https://doi.org/10.1021/jp1011457.
[24] Wang, J. Yu, R. Zhu, J. Zhu, A.T. Smith, H. He, D. O'Hare, L. Sun, Functionovative applicationalized layered double hydroxides for inns, Mater. Horizons. 7 (2020) 715–745. https://doi.org/10.1039/C9MH01494B.
[25] J. He, M. Wei, B. Li, Y. Kang, D.G. Evans, X. Duan, Preparation of Layered Double Hydroxides, in: Layer. Double Hydroxides, Springer-Verlag, Berlin/Heidelberg, 2006: pp. 89–119. https://doi.org/10.1007/430_006.
[26] V. Rives, M. del Arco, C. Martín, Intercalation of drugs in layered double hydroxides and their controlled release: A review, Appl. Clay Sci. 88–89 (2014) 239–269. https://doi.org/10.1016/j.clay.2013.12.002.
[27] S. Radha, P.V. Kamath, Polytype selection and structural disorder mediated by intercalated sulfate ions among the layered double hydroxides of Zn with Al and Cr, Cryst. Growth Des. 9 (2009) 3197–3203. https://doi.org/10.1021/cg801259n.
[28] X. Duan, J. Lu, D.G. Evans, X. Wei, J.S. Chen, Functional Host–Guest Materials, in: Mod. Inorg. Synth. Chem., Elsevier, 2017: pp. 493–543. https://doi.org/10.1016/B978-0-444-63591-4.00018-5.
[29] S. Marappa, S. Radha, P.V. Kamath, Nitrate-Intercalated Layered Double Hydroxides - Structure Model, Order, and Disorder, Eur. J. Inorg. Chem. 2013 (2013) 2122–2128. https://doi.org/10.1002/ejic.201201405.
[30] S. Radha, S. V. Prasanna, P.V. Kamath, Polytype selection by intercalated anions: Design and synthesis of the 3R2 polytype of the layered double hydroxide of Zn and Al, Cryst. Growth Des. 11 (2011) 2287–2293. https://doi.org/10.1021/cg101707n.
[31] J. Wang, T. Zhang, M. Li, Y. Yang, P. Lu, P. Ning, Q. Wang, Arsenic removal from water/wastewater using layered double hydroxide derived adsorbents, a critical review, RSC Adv. 8 (2018) 22694–22709. https://doi.org/10.1039/c8ra03647k.
[32] V. Rives, M. Del Arco, C. Martín, Layered double hydroxides as drug carriers and for controlled release of non-steroidal antiinflammatory drugs (NSAIDs): A review, J. Control. Release. 169 (2013) 28–39. https://doi.org/10.1016/j.jconrel.2013.03.034.
[33] M. V. Bukhtiyarova, A review on effect of synthesis conditions on the formation of layered double hydroxides, J. Solid State Chem. 269 (2019) 494–506. https://doi.org/10.1016/j.jssc.2018.10.018.
[34] L. Mohapatra, K. Parida, A review on the recent progress, challenges and perspective of layered double hydroxides as promising photocatalysts, J. Mater. Chem. A. 4 (2016) 10744–10766. https://doi.org/10.1039/c6ta01668e.
[35] S. Radha, A. Navrotsky, Energetics of CO2 adsorption on mg-al layered double hydroxides and related mixed metal oxides, J. Phys. Chem. C. 118 (2014) 29836–29844. https://doi.org/10.1021/jp508678k.

[36] M.P. Browne, Z. Sofer, M. Pumera, Layered and two dimensional metal oxides for electrochemical energy conversion, Energy Environ. Sci. 12 (2019) 41–58. https://doi.org/10.1039/c8ee02495b.
[37] N. Baliarsingh, K.M. Parida, G.C. Pradhan, Influence of the nature and concentration of precursor metal ions in the brucite layer of LDHs for phosphate adsorption-a review, RSC Adv. 3 (2013) 23865–23878. https://doi.org/10.1039/c3ra42857e.
[38] M. Daud, A. Hai, F. Banat, M.B. Wazir, M. Habib, G. Bharath, M.A. Al-Harthi, A review on the recent advances, challenges and future aspect of layered double hydroxides (LDH)–Containing hybrids as promising adsorbents for dyes removal, J. Mol. Liq. 288 (2019) 110989. https://doi.org/10.1016/j.molliq.2019.110989.
[39] S. Radha, A. Navrotsky, Energetics of CO2 Adsorption on Mg–Al Layered Double Hydroxides and Related Mixed Metal Oxides, J. Phys. Chem. C. 118 (2014) 29836–29844. https://doi.org/10.1021/jp508678k.
[40] K. Takehira, Recent development of layered double hydroxide-derived catalysts − Rehydration, reconstitution, and supporting, aiming at commercial application −, Appl. Clay Sci. 136 (2017) 112–141. https://doi.org/10.1016/j.clay.2016.11.012.
[41] J. Rocha, V. Rives, M.A. Ulibarri, Reconstruction of layered double hydroxides from calcined precursors: a powder XRD and 27 Al MAS NMR study, 3 (1999) 2499–2503.
[42] B. Kutlu, A. Leuteritz, R. Boldt, D. Jehnichen, G. Heinrich, Effects of LDH synthesis and modification on the exfoliation and introduction of a robust anion-exchange procedure, Chem. Eng. J. 243 (2014) 394–404. https://doi.org/10.1016/j.cej.2014.01.026.
[43] N. Chubar, V. Gerda, O. Megantari, M. Mičušík, M. Omastova, K. Heister, P. Man, J. Fraissard, Applications versus properties of Mg-Al layered double hydroxides provided by their syntheses methods: Alkoxide and alkoxide-free sol-gel syntheses and hydrothermal precipitation, Chem. Eng. J. 234 (2013) 284–299. https://doi.org/10.1016/j.cej.2013.08.097.
[44] F.L. Theiss, G.A. Ayoko, R.L. Frost, Synthesis of layered double hydroxides containing Mg 2+ , Zn 2+ , Ca 2+ and Al 3+ layer cations by co-precipitation methods - A review, Appl. Surf. Sci. 383 (2016) 200–213. https://doi.org/10.1016/j.apsusc.2016.04.150.
[45] Z. Chang, D.G. Evans, X. Duan, C. Vial, J. Ghanbaja, V. Prevot, M. De Roy, C. Forano, Synthesis of [Zn-Al-CO3] layered double hydroxides by a coprecipitation method under steady-state conditions, J. Solid State Chem. 178 (2005) 2766–2777. https://doi.org/10.1016/j.jssc.2005.06.024.
[46] E. Conterosito, V. Gianotti, L. Palin, E. Boccaleri, D. Viterbo, M. Milanesio, Facile preparation methods of hydrotalcite layered materials and their structural characterization by combined techniques, Inorganica Chim. Acta. 470 (2018) 36–50. https://doi.org/10.1016/j.ica.2017.08.007.
[47] M.R. Othman, Z. Helwani, Martunus, W.J.N. Fernando, Synthetic hydrotalcites from different routes and their application as catalysts and gas adsorbents: a review, Appl. Organomet. Chem. 23 (2009) 335–346. https://doi.org/10.1002/aoc.1517.
[48] C. Del Hoyo, Layered double hydroxides and human health: An overview, Appl. Clay Sci. 36 (2007) 103–121. https://doi.org/10.1016/j.clay.2006.06.010.
[49] W.H. Zhang, X.D. Guo, J. He, Z.Y. Qian, Preparation of Ni(II)/Ti(IV) layered double hydroxide at high supersaturation, J. Eur. Ceram. Soc. 28 (2008) 1623–1629. https://doi.org/10.1016/j.jeurceramsoc.2007.11.016.
[50] E.L. Crepaldi, P.C. Pavan, J.B. Valim, Comparative Study of the Coprecipitation Methods for the Preparation of Layered Double Hydroxides, (2000) 64–70.
[51] J. Bauer, P. Behrens, M. Speckbacher, H. Langhals, Composites of Perylene Chromophores and Layered Double Hydroxides: Direct Synthesis, Characterization, and Photo- and Chemical Stability, Adv. Funct. Mater. 13 (2003) 241–248. https://doi.org/10.1002/adfm.200390036.
[52] M. Del Arco, E. Cebadera, S. Gutiérrez, C. Martín, M.J. Montero, V. Rives, J. Rocha, M.A. Sevilla, Mg,Al layered double hydroxides with intercalated indomethacin: Synthesis, characterization, and pharmacological study, J. Pharm. Sci. 93 (2004) 1649–1658. https://doi.org/10.1002/jps.20054.

[53] N. Chubar, R. Gilmour, V. Gerda, M. Mičušík, M. Omastova, K. Heister, P. Man, J. Fraissard, V. Zaitsev, Layered double hydroxides as the next generation inorganic anion exchangers: Synthetic methods versus applicability, Adv. Colloid Interface Sci. 245 (2017) 62–80. https://doi.org/10.1016/j.cis.2017.04.013.
[54] J.S. Valente, M.S. Cantú, J.G.H. Cortez, R. Montiel, X. Bokhimi, E. López-Salinas, Preparation and characterization of sol-gel MgAl hydrotalcites with nanocapsular morphology, J. Phys. Chem. C. 111 (2007) 642–651. https://doi.org/10.1021/jp065283h.
[55] O. Lorret, S. Morandi, F. Prinetto, G. Ghiotti, D. Tichit, R. Durand, B. Coq, Synthesis and characterization of Pt/Mg(Al)O catalysts obtained from layered double hydroxides by different routes, Microporous Mesoporous Mater. 103 (2007) 48–56. https://doi.org/10.1016/j.micromeso.2007.01.035.
[56] T. Lopez, P. Bosch, E. Ramos, R. Gomez, O. Novaro, | D Acosta, F. Figueras, Synthesis and Characterization of Sol-Gel Hydrotalcites. Structure and Texture †, 1996. https://pubs.acs.org/sharingguidelines (accessed April 30, 2020).
[57] S.P. Paredes, G. Fetter, P. Bosch, S. Bulbulian, Sol-gel synthesis of hydrotalcite - Like compounds, J. Mater. Sci. 41 (2006) 3377–3382. https://doi.org/10.1007/s10853-005-5347-4.
[58] M.A. Aramendía, V. Borau, C. Jiménez, J.M. Marinas, J.R. Ruiz, F.J. Urbano, Comparative study of Mg/M(III) (M=Al, Ga, In) layered double hydroxides obtained by coprecipitation and the sol-gel method, J. Solid State Chem. 168 (2002) 156–161. https://doi.org/10.1006/jssc.2002.9655.
[59] L.A. Utracki, M. Sepehr, E. Boccaleri, Synthetic, layered nanoparticles for polymeric nanocomposites (PNCs), Polym. Adv. Technol. 18 (2007) 1–37. https://doi.org/10.1002/pat.852.
[60] Z. Yang, H. Peng, W. Wang, T. Liu, Crystallization behavior of poly(ε-caprolactone)/layered double hydroxide nanocomposites, J. Appl. Polym. Sci. 116 (2010) 2658–2667. https://doi.org/10.1002/app.
[61] B. Kutlu, A. Leuteritz, R. Boldt, D. Jehnichen, G. Heinrich, Effects of LDH synthesis and modification on the exfoliation and introduction of a robust anion-exchange procedure, Chem. Eng. J. 243 (2014) 394–404. https://doi.org/10.1016/j.cej.2014.01.026.
[62] G. Mishra, B. Dash, S. Pandey, Layered double hydroxides: A brief review from fundamentals to application as evolving biomaterials, Appl. Clay Sci. 153 (2018) 172–186. https://doi.org/10.1016/j.clay.2017.12.021.
[63] J. Wan, S.D. Lacey, J. Dai, W. Bao, M.S. Fuhrer, L. Hu, Tuning two-dimensional nanomaterials by intercalation: Materials, properties and applications, Chem. Soc. Rev. 45 (2016) 6742–6765. https://doi.org/10.1039/c5cs00758e.
[64] S. Ma, L. Huang, L. Ma, Y. Shim, S.M. Islam, P. Wang, L.D. Zhao, S. Wang, G. Sun, X. Yang, M.G. Kanatzidis, Efficient Uranium Capture by Polysulfide/Layered Double Hydroxide Composites, J. Am. Chem. Soc. 137 (2015) 3670–3677. https://doi.org/10.1021/jacs.5b00762.
[65] F. Cavani, F. Trifirò, A. Vaccari, Hydrotalcite-type anionic clays: Preparation, properties and applications., Catal. Today. 11 (1991) 173–301. https://doi.org/10.1016/0920-5861(91)80068-K.
[66] S.J. Xia, Z.M. Ni, Q. Xu, B.X. Hu, J. Hu, Layered double hydroxides as supports for intercalation and sustained release of antihypertensive drugs, J. Solid State Chem. 181 (2008) 2610–2619. https://doi.org/10.1016/j.jssc.2008.06.009.
[67] L. Perioli, C. Pagano, Inorganic matrices: An answer to low drug solubility problem, Expert Opin. Drug Deliv. 9 (2012) 1559–1572. https://doi.org/10.1517/17425247.2012.733693.
[68] V. Rives, M. del Arco, C. Martín, Intercalation of drugs in layered double hydroxides and their controlled release: A review, Appl. Clay Sci. 88–89 (2014) 239–269. https://doi.org/10.1016/j.clay.2013.12.002.
[69] J. Wang, Q. Liu, G. Zhang, Z. Li, P. Yang, X. Jing, M. Zhang, T. Liu, Z. Jiang, Synthesis, sustained release properties of magnetically functionalized organic-inorganic materials: Amoxicillin anions intercalated magnetic layered double hydroxides via calcined precursors at room temperature, Solid State Sci. 11 (2009) 1597–1601. https://doi.org/10.1016/j.solidstatesciences.2009.06.015.

[70] S. Zhang, J. Liu, P. Huang, H. Wang, C. Cao, W. Song, Carbonaceous aerogel and CoNiAl-LDH@CA nanocomposites derived from biomass for high performance pseudo-supercapacitor, Sci. Bull. 62 (2017) 841–845. https://doi.org/10.1016/j.scib.2017.05.019.
[71] Y. Zhao, Q. Wang, T. Bian, H. Yu, H. Fan, C. Zhou, L.-Z. Wu, C.-H. Tung, D. O'hare, T. Zhang, Ni 3+ doped monolayer layered double hydroxide nanosheets as efficient electrodes for supercapacitors †, Nanoscale. 7 (2015) 7168. https://doi.org/10.1039/c5nr01320h.
[72] Y. Zhao, B. Li, Q. Wang, W. Gao, C.J. Wang, M. Wei, D.G. Evans, X. Duan, D. O'Hare, NiTi-Layered double hydroxides nanosheets as efficient photocatalysts for oxygen evolution from water using visible light, Chem. Sci. 5 (2014) 951–958. https://doi.org/10.1039/c3sc52546e.
[73] J.-M. Oh, S.-J. Choi, G.-E. Lee, S.-H. Han, J.-H. Choy, Inorganic Drug-Delivery Nanovehicle Conjugated with Cancer-Cell-Specific Ligand, Adv. Funct. Mater. 19 (2009) 1617–1624. https://doi.org/10.1002/adfm.200801127.
[74] C. Del Hoyo, Layered double hydroxides and human health: An overview, Appl. Clay Sci. 36[1] C. D (2007) 103–121. https://doi.org/10.1016/j.clay.2006.06.010.
[75] U. Costantino, M. Nocchetti, L. Tammaro, V. Vittoria, Modified Hydrotalcite–Like Compounds as Active Fillers of Biodegradable Polymers for Drug Release and Food Packaging Applications, Recent Pat. Nanotechnol. 6 (2012) 218–230. https://doi.org/10.2174/187221012803531493.
[76] Y. Kuthati, R.K. Kankala, C.H. Lee, Layered double hydroxide nanoparticles for biomedical applications: Current status and recent prospects, Appl. Clay Sci. 112–113 (2015) 100–116. https://doi.org/10.1016/j.clay.2015.04.018.
[77] C. Taviot-Guého, V. Prévot, C. Forano, G. Renaudin, C. Mousty, F. Leroux, Tailoring Hybrid Layered Double Hydroxides for the Development of Innovative Applications, Adv. Funct. Mater. 28 (2018) 1–33. https://doi.org/10.1002/adfm.201703868.
[78] S.J. Ryu, H. Jung, J.M. Oh, J.K. Lee, J.H. Choy, Layered double hydroxide as novel antibacterial drug delivery system, J. Phys. Chem. Solids. (2010). https://doi.org/10.1016/j.jpcs.2009.12.066.
[79] V. Ambrogi, L. Perioli, V. Ciarnelli, M. Nocchetti, C. Rossi, Effect of gliclazide immobilization into layered double hydroxide on drug release, Eur. J. Pharm. Biopharm. 73 (2009) 285–291. https://doi.org/10.1016/j.ejpb.2009.06.007.
[80] L. Yan, S. Gonca, G. Zhu, W. Zhang, X. Chen, Layered double hydroxide nanostructures and nanocomposites for biomedical applications, J. Mater. Chem. B. 7 (2019) 5583–5601. https://doi.org/10.1039/c9tb01312a.
[81] K. Ladewig, P.X. Zhi, Q.L. Gao, Layered double hydroxide nanoparticles in gene and drug delivery, Expert Opin. Drug Deliv. 6 (2009) 907–922. https://doi.org/10.1517/17425240903130585.
[82] G.N. Pshinko, Layered Double Hydroxides as Effective Adsorbents for U(VI) and Toxic Heavy Metals Removal from Aqueous Media, J. Chem. 2013 (2013). https://doi.org/10.1155/2013/347178.
[83] H. Asiabi, Y. Yamini, M. Shamsayei, E. Tahmasebi, Highly selective and efficient removal and extraction of heavy metals by layered double hydroxides intercalated with the diphenylamine-4-sulfonate: A comparative study, Chem. Eng. J. 323 (2017) 212–223. https://doi.org/10.1016/j.cej.2017.04.096.
[84] D. Banerjee, D. Kim, M.J. Schweiger, A.A. Kruger, P.K. Thallapally, Removal of TcO4- ions from solution: Materials and future outlook, Chem. Soc. Rev. 45 (2016) 2724–2739. https://doi.org/10.1039/c5cs00330j.
[85] R. Borges, F. Wypych, E. Petit, C. Forano, V. Prevot, Potential sustainable slow-release fertilizers obtained by mechanochemical activation of MgAl and MgFe layered double hydroxides and K 2 HPO 4, Nanomaterials. 9 (2019). https://doi.org/10.3390/nano9020183.
[86] D. Zhao, C. Wang, F. Yu, Y. Shi, P. Cao, J. Dan, K. Chen, Y. Lv, X. Guo, B. Dai, Enhanced oxygen vacancies in a two-dimensional MnAl-layered double oxide prepared via flash nanoprecipitation offers high selective catalytic reduction of NOx with NH3, Nanomaterials. 8 (2018). https://doi.org/10.3390/nano8080620.

[87] J. Feng, Y. He, Y. Liu, Y. Du, D. Li, Supported catalysts based on layered double hydroxides for catalytic oxidation and hydrogenation: general functionality and promising application prospects, Chem. Soc. Rev. 44 (2015) 5291–5319. https://doi.org/10.1039/c5cs00268k.
[88] S. Tonda, W.K. Jo, Plasmonic Ag nanoparticles decorated NiAl-layered double hydroxide/graphitic carbon nitride nanocomposites for efficient visible-light-driven photocatalytic removal of aqueous organic pollutants, Catal. Today. 315 (2018) 213–222. https://doi.org/10.1016/j.cattod.2017.12.019.
[89] Q. Wang, D. Ohare, Recent advances in the synthesis and application of layered double hydroxide (LDH) nanosheets, Chem. Rev. 112 (2012) 4124–4155. https://doi.org/10.1021/cr200434v.
[90] J. Yang, C. Yu, X. Fan, J. Qiu, 3D Architecture Materials Made of NiCoAl-LDH Nanoplates Coupled with NiCo-Carbonate Hydroxide Nanowires Grown on Flexible Graphite Paper for Asymmetric Supercapacitors, Adv. Energy Mater. 4 (2014) 1400761. https://doi.org/10.1002/aenm.201400761.
[91] A. Smalenskaite, A.N. Salak, M.G.S. Ferreira, R. Skaudzius, A. Kareiva, Sol-gel synthesis and characterization of hybrid inorganic-organic Tb(III)-terephthalate containing layered double hydroxides, Opt. Mater. (Amst). 80 (2018) 186–196. https://doi.org/10.1016/j.optmat.2018.04.048.

SUMMARY

VILNIUS UNIVERSITY
FACULTY OF CHEMISTRY AND GEOSCIENCES

MYKHAILO SULEIMANOV

Investigation of substitution effects in layered double hydroxides

By using sol-gel synthesis method alkaline earth metal substituted layered double hydroxides (LDHs) of $Mg_{2-x}M_x/Al_1$ (M = Ca, Sr, Ba) were fabricated. Related MMO were obtained by calcination of $Mg_{2-x}Ca_x/Al_1$ LDHs precursor gels at 650°C. The substitution effects were investigated by changing the amount and nature of the introduced alkaline earth metals. After reconstruction mixed-metal LDH samples were intercalated with citrate and tartrate anions via the anion-exchange method. The X-ray powder diffraction (XRD) analysis confirmed successful intercalation of anions into host LDHs by indicating the growth of interlayer distance. The synthesis materials were characterized using XRD, infrared spectroscopy (FT-IR) and scanning electron microscopy (SEM). The specific surface area and pore size of differently substituted $Mg_{2-x}M_x/Al_1$ LDH samples were estimated by BJH and BET methods. Obtained results demonstrated that the nature and the amount of earth-alkaline metal affect the surface properties, morphological features and purity of substituted metal-mixed LDHs. The synthesized LDH materials could be tested for different biomedical applications and could be used as precursor materials for the preparation of drug delivery systems.